The Astrophysical Journal Supplement Series, 199:28 (17pp), 2012 April doi:10.1088/0067-0049/199/2/28

A REMARKABLE LONG-TERM LIGHT CURVE AND DEEP, LOW-STATE SPECTROSCOPY: *SWIFT* AND *XMM-NEWTON* MONITORING OF THE NLS1 GALAXY Mkn 335

Dirk Grupe[1], S. Komossa[2,3,4], Luigi C. Gallo[5], Anna Lia Longinotti[6,7], Andrew C. Fabian[8], Anil K. Pradhan[9], Michael Gruberbauer[5], and Dawei Xu[10]

[1] Department of Astronomy and Astrophysics, Pennsylvania State University, 525 Davey Lab, University Park, PA 16802, USA; grupe@astro.psu.edu
[2] Technische Universität München, Fakultät für Physik, James-Franck-Strasse 1/I, D-85748 Garching, Germany; stefanie.komossa@gmx.de
[3] Excellence Cluster Universe, TUM, Boltzmannstrasse 2, D-85748 Garching, Germany
[4] Max Planck Institut für Plasmaphysik, Boltzmannstrasse 2, D-85748 Garching, Germany
[5] Department of Astronomy and Physics, Saint Mary's University, Halifax, NS B3H 3C3, Canada; lgallo@ap.stmarys.ca
[6] MIT Kavli Institute for Astrophysics and Space Research, 77 Massachusetts Avenue, NE80-6011 Cambridge, MA 02139, USA
[7] XMM-Newton Science Operations Centre, ESAC, P.O. Box 78, 28691 Villanueva de la Cañada, Madrid, Spain
[8] Institute of Astronomy, Madingley Road, Cambridge, CB3 0HA, UK
[9] Department of Astronomy, The Ohio State University, 140 West 18th Avenue, Columbus, OH 43210, USA; pradhan@astronomy.ohio-state.edu
[10] National Astronomical Observatories, Chinese Academy of Sciences, 20A Datun Road, Beijing 100012, China; dwxu@nao.cas.cn
Received 2011 July 15; accepted 2012 January 23; published 2012 March 27

ABSTRACT

The narrow-line Seyfert 1 galaxy (NLS1) Mkn 335 is remarkable because it has repeatedly shown deep, long X-ray low states that show pronounced spectral structure. It has become one of the prototype active galactic nuclei (AGNs) in deep minimum X-ray states. Here we report on the continuation of our ongoing monitoring campaign with *Swift* and the examination of the low-state X-ray spectra based on a 200 ks triggered observation with *XMM-Newton* in 2009 June. *Swift* has continuously monitored Mkn 335 since 2007 May typically on a monthly basis. This is one of the longest simultaneous UV/X-ray light curves so far obtained for an AGN. Mkn 335 has shown strong X-ray variability even on timescales of hours. In the UV, it turns out to be one of the most variable among NLS1s. Long-term *Swift* monitoring allows us to examine correlations between the UV, X-rays, and X-ray hardness ratios. We find no significant correlation or lag between the UV and X-ray variability; however, we do find distinct trends in the behavior of the hardness ratio variability. The hardness ratio and count rate are correlated in the low-flux state, but no correlation is seen in the high state. The X-ray low-state spectra of the 2007 and 2009 *XMM-Newton* observations display significant spectral variability. We fit the X-ray spectra with a suite of phenomenological models in order to characterize the data. The broadband CCD spectrum can be fitted equally well with partial absorption and blurred reflection models. These more complicated models are explored in further detail in upcoming work.

Key words: galaxies: active – galaxies: individual (Mkn 335) – galaxies: Seyfert – X-rays: galaxies

Online-only material: color figures

1. INTRODUCTION

While active galactic nuclei (AGNs) typically vary in X-rays by factors of a few (e.g., Grupe et al. 2001), some AGNs show dramatic drops in their X-ray flux, accompanied by changes in their spectrum. These AGNs are known to be typically X-ray bright, but for some time they display very low flux states which makes them different from AGNs such as PHL 1811 which are intrinsically X-ray weak (Leighly et al. 2007). Some recent examples of such deep minimum states observed in AGNs are PG 2112+059, PG 1535+547, PG 1543+489, RX J2217.9–5941, Mkn 335, PHL 1092, and PG 0844+349 (Schartel et al. 2010, 2007; Ballo et al. 2008; Vignali et al. 2008; Grupe et al. 2004a, 2004b, 2007a, 2008a; Miniutti et al. 2009; Gallo et al. 2011). Absorption has always been considered to play an important role in explaining AGN X-ray spectra. Variability through a variable absorber may play a much more important role in AGNs than previously thought (e.g., Turner & Miller 2009). Some of the best examples of variable absorbers are, e.g., NGC 1365 (Risaliti et al. 2009), Mkn 766 (Miller et al. 2007; Turner et al. 2007), 1H 0557–385 (Longinotti et al. 2009), and NGC 3516 (Turner et al. 2011).

However, this picture is far from being complete and clear. Besides absorption, a popular explanation of the X-ray low states in AGNs are reflection models such as proposed by Fabian et al. (2002, 2004, 2009) for 1H 0707–495, or by Gallo (2006) for NLS1s in general. Both reflection and partial covering absorber models produce relatively similar X-ray spectra (see, e.g., discussion in Grupe et al. 2008a). To make things even more complex, as shown by, e.g., Chevalier et a. (2006) and Merloni et al. (2006), the X-ray spectrum can be dominated in the high state by reflection and is then modified by a partial covering absorber when the AGN is in a low state. Even for MCG-6-30-15, which has been the poster child for reflection models after the *ASCA* detection of a broad red wing of the Fe Kα line by Tanaka et al. (1995), Miller et al. (2008, 2009) argued that its X-ray spectra can be consistently explained by partial covering absorption.

Bright AGNs in deep low states with well-covered light curves and good low-state spectra are essential for further exploring the physics which are responsible for the structures and features seen in AGN X-ray spectra, and especially in low states, where spectral complexity is most pronounced. The narrow-line Seyfert 1 galaxy (NLS1) Mkn 335 ($\alpha_{2000} = 00^{h}06^{m}19\overset{s}{.}5$, $\delta_{2000} = +20^{\circ}12'11\overset{''}{.}0$) is such an AGN: it goes repeatedly into deep low states, is relatively X-ray bright even in those states, and has been monitored by us for years to identify these low states. It shows interesting spectral structures, and one possible interpretation has been that it exhibits an unusually broad Fe line (Longinotti et al. 2007a). It is nearby ($z = 0.0258$), well studied in the optical spectral band, and has a well-measured black hole mass of $1.4 \times 10^7\ M_\odot$ from reverberation mapping (Peterson et al. 2004; Grier et al. 2012).

Mkn 335 has been known to be an X-ray bright AGN for decades, starting with *UHURU* (Tananbaum et al. 1978) and *EINSTEIN* (Halpern 1982). *EXOSAT* and BBXRT observations suggested a strong soft X-ray excess in the X-ray spectrum of Mkn 335 (Pounds et al. 1987 and Turner et al. 1993, respectively) while Nandra & Pounds (1994) reported on the presence of a warm absorber in this source. During the *ROSAT* All-Sky Survey and pointed observations, Mkn 335 appeared to be X-ray bright, and was modeled with a strong soft X-ray excess (Grupe et al. 2001). From the 1993 observations by *ASCA* (George et al. 2000), Leighly (1999) concluded that the X-ray spectrum was affected by the presence of a warm absorber, while Ballantyne et al. (2001) interpreted the spectral shape by X-ray reflection on the accretion disk. Mkn 335 was also observed by *XMM-Newton* in 2000 and 2006 (Gondoin et al. 2002; Longinotti et al. 2007a, 2007b; O'Neill et al. 2007; Arevalo et al. 2008) and *Suzaku* in 2006 June (Larsson et al. 2008). In all cases, Mkn 335 was X-ray bright, with the exception of one *EXOSAT* observation in 1983 (Pounds et al. 1987).

However, when Mkn 335 was observed by *Swift* (Gehrels et al. 2004) in 2007 May as part of a *Swift* fill in project to study the spectral energy distributions in AGNs (Grupe et al. 2010), it appeared to be dramatically fainter in X-rays than expected from previous X-ray observations (Grupe et al. 2007a). In order to investigate the nature of the low state in more detail, we initiated a Target-of-Opportunity (ToO) observation with *XMM-Newton*, which was executed on 2007 July 10 (Grupe et al. 2008a). During this 22 ks *XMM-Newton* observation, we discovered strong soft X-ray emission lines of H and He-like ions such as O VII (Grupe et al. 2008a; Longinotti et al. 2008) in the Reflection Grating Spectrometer (RGS; den Herder et al. 2001). These lines are only visible during an extreme X-ray low state and they can provide information of the physical conditions of the gas surrounding the central black hole. Because the 22 ks *XMM-Newton* observation was too short to obtain any reliable line ratios, we applied for a 200 ks *XMM-Newton* observation which would be triggered by a low state seen by *Swift*. When *Swift* started the monitoring campaign again in 2009 May after Mkn 335 came out of the Sun constraint, it appeared to be again in an extreme low state. We therefore triggered our approved *XMM-Newton* observation and observed Mkn 335 for 200 ks in 2009 June11–14. Mkn 335 also became a target of our *Swift* Guest Investigator program in 2008 in which we monitored the AGN on a weekly basis in X-rays and all six UVOT filters.

Here we report on the results of the *Swift* monitoring campaign of Mkn 335 and the continuum short-term light curve measured by *XMM-Newton* during the 200 ks triggered observation. This first paper in a sequence focuses on presenting the rich data sets, on simple modeling, and on revealing spectral trends. In-depth modeling of the multi-component warm absorber based on the RGS data, and a detailed investigation of blurred reflection models will each be presented in follow-up work. This paper is organized as follows: in Section 2, we describe the observations and the data reduction of the *Swift* and *XMM-Newton* observations. In Section 3, we present the long- and short-term light curves and the analysis of the X-ray spectra obtained by *XMM-Newton*. The results of this analysis are discussed in Section 4. Throughout the paper spectral indices are denoted as energy spectral indices with $F_\nu \propto \nu^{-\alpha}$. Luminosities are calculated assuming a ΛCDM cosmology with $\Omega_{\rm M} = 0.27$, $\Omega_\Lambda = 0.73$ and a Hubble constant of $H_0 = 75$ km s^{-1} Mpc^{-1} corresponding to a luminosity distance $D = 105$ Mpc. All errors are 90% confidence unless stated otherwise.

2. OBSERVATIONS AND DATA REDUCTION

2.1. *Swift* Observations

Swift started monitoring Mkn 335 on 2007 May 17 and still continues with this campaign on at least a monthly basis (Table 1), except for the period of February to May when Mkn 335 is in Sun constraint for *Swift*. As part of a *Swift* Guest Investigator program, the cadence was changed to once per week starting in 2008 June. The X-Ray Telescope (XRT; Burrows et al. 2005) observations were performed in Photon Counting mode (PC mode; Hill et al. 2004). X-ray data were reduced with the task *xrtpipeline* version 0.12.1. Source and background photons were extracted with *XSELECT* version 2.4, from circles with radii of 47″ and 189″, respectively, when the source count rate was less than 0.4 counts s^{-1}. However, during some parts of our monitoring campaign the count rates were significantly higher than 0.4 counts s^{-1}, which means that the data were affected by pileup. In order to avoid the effects of pileup we excluded the inner part of the point-spread function, depending on the brightness of the AGN. The spectral data were rebinned with at least 20 photons bin^{-1} using *grppha* version 3.0.0. The 0.3–10.0 keV spectra were analyzed with *XSPEC* version 12.3.1x (Arnaud 1996). The auxiliary response files were created with *xrtmkarf* and corrected using the exposure maps, and the standard response matrices *swxpc0to12s0_20010101v011.rmf* and *swxpc0to12s6_20010101v011.rmf* were used for the observations before and after the XRT substrate voltage change in 2007 August, respectively (Godet et al. 2009).

The UV-optical Telescope (UVOT; Roming et al. 2005) covers the range between 1700 and 6500 Å and is a sister instrument of *XMM-Newton*'s Optical Monitor (OM). Although it has a similar set of filters to the OM (Mason et al. 2001; Roming et al. 2005), the UVOT UV throughput is a factor of about 10 higher than that of the OM. The UVOT data were co-added for each segment in each filter with the UVOT task *uvotimsum* version 1.3. Source photons in all filters were selected in a circle with a radius of 5″. UVOT magnitudes and fluxes were measured with the task *uvotsource* version 3 based on the most recent UVOT calibration as described in Poole et al. (2008) and Breeveld et al. (2010). The UVOT data were corrected for Galactic reddening ($E_{\rm B-V} = 0.035$; Schlegel et al. 1998). The correction factor in each filter was calculated with Equation (2) in Roming et al. (2009) who used the standard reddening correction curves by Cardelli et al. (1989).

2.2. *XMM-Newton* Observations

We observed Mkn 335 with *XMM-Newton* (Jansen et al. 2001) on 2009 June 11–14 for a total of 200 ks split over orbits 1741 and 1742. A summary of the observations with each of the instruments on board *XMM-Newton* is given in Table 2. The European Photon Imaging Camera (EPIC) pn (Strüder et al. 2001) was operated in Large Window mode with the thin filter. This combination was chosen to avoid pileup in case the AGN re-brightened. The two EPIC MOS (Turner et al. 2001) were both operated in Full-Frame mode with the medium filters. High-resolution X-ray spectroscopy was performed using the two RGSs (den Herder et al. 2001) on board *XMM-Newton*.

Table 1
Swift Observation Log of Mkn 335

ObsID	Segment	*T*-start[a]	*T*-stop[a]	MJD[b]	T_{XRT}[c]	T_V[3c]	T_B[c]	T_U[c]	T_{UVW1}[c]	T_{UVM2}[c]	T_{UVW2}[c]
35755	001	2007 May 17 00:32	2007 May 17 05:37	54237.128	4859	401	401	401	800	1082	1603
	002	2007 May 25 00:01	2007 May 25 19:23	54245.406	8084	658	658	658	1323	1677	2648
	003	2007 Jun 28 00:01	2007 Jun 28 14:37	54279.073	2932	273	273	273	545	677	1092
	004	2007 Jun 30 00:13	2007 Jun 30 14:52	54281.314	2837	230	230	230	461	615	921
	005	2007 Jul 2 14:47	2007 Jul 2 21:18	54283.751	2979	245	245	245	490	614	983
	008	2007 Sep 19 00:05	2007 Sep 19 11:24	54362.219	1389	...	...	...	...	...	...
	009	2007 Sep 25 00:55	2007 Sep 25 05:51	54368.141	2050	...	...	...	...	...	...
	010	2007 Oct 4 00:01	2007 Oct 4 03:13	54377.068	1401	...	...	...	...	...	...
	011	2007 Oct 7 14:56	2007 Oct 7 23:13	54380.795	3326	...	...	...	...	...	...
	012	2007 Oct 8 15:02	2007 Oct 8 23:19	54381.799	3314	...	...	...	...	...	...
	013	2007 Oct 9 05:32	2007 Oct 9 21:44	54382.569	4869	...	...	...	...	...	...
	014	2007 Oct 10 05:33	2007 Oct 10 21:46	54383.569	3583	...	...	...	...	...	...
	015	2007 Oct 11 01:05	2007 Oct 11 23:36	54384.514	3898	...	...	...	...	...	...
	016	2007 Oct 12 05:51	2007 Oct 13 22:10	54386.084	9173	...	...	...	...	...	...
	017	2007 Oct 17 00:01	2007 Oct 17 09:27	54390.198	3518	...	...	...	...	...	...
	018	2007 Oct 18 01:20	2007 Oct 18 14:21	54391.327	4531	...	...	...	...	...	...
	019	2007 Oct 19 04:51	2007 Oct 20 19:20	54393.000	12332	...	...	...	...	...	...
	020	2007 Oct 21 03:25	2007 Oct 22 14:41	54394.899	2719	...	...	...	...	...	...
	021	2007 Oct 31 12:47	2007 Oct 31 24:00	54404.766	2020	170	171	171	431	204	682
	022	2007 Dec 5 01:19	2007 Dec 5 07:59	54439.194	5032	412	412	412	826	1136	1650
	023	2007 Dec 12 11:55	2007 Dec 12 13:48	54446.536	1952	160	160	160	320	439	643
	024	2007 Dec 19 20:29	2001 Dec 19 22:13	54453.890	1883	150	150	150	300	410	601
	025	2007 Dec 26 13:08	2007 Dec 26 15:00	54460.586	1846	151	151	151	302	412	605
	026	2008 Jan 2 07:17	2008 Jan 2 12:06	54467.404	2700	222	222	222	442	535	887
	027	2008 Jan 9 20:51	2008 Jan 9 24:00	54474.935	2143	175	175	175	350	468	702
90006	001	2008 Jun 1 13:54	2008 Jan 1 15:49	54618.619	2108	171	171	171	342	492	685
	002	2008 Jun 8 00:35	2008 Jun 8 03:58	54625.095	2185	187	187	187	375	421	751
	003	2008 Jun 15 00:48	2008 Jun 15 02:45	54632.074	2323	200	200	200	401	447	803
	004	2008 Jun 22 00:17	2008 Jun 22 22:59	54639.484	8104	675	675	675	1352	1708	2707
	005	2008 Jun 29 13:45	2008 Jun 29 17:16	54646.645	2376	192	192	192	385	524	771
	006	2008 Jul 5 23:43	2008 Jul 6 01:43	54653.030	2153	110	210	210	421	296	838
	007	2008 Jul 13 21:41	2008 Jul 13 23:31	54660.909	1201	102	102	102	204	240	409
	008	2008 Jul 20 01:34	2008 Jul 20 06:21	54667.165	1546	56	169	169	340	118	629
	009	2008 Jul 27 08:26	2008 Jul 27 10:17	54674.390	1795	159	171	171	342	209	685
	010	2008 Aug 3 12:13	2008 Aug 3 13:49	54681.542	2043	169	171	171	342	451	681
	011	2008 Aug 10 13:03	2008 Aug 10 16:29	54688.615	1928	131	182	182	366	390	703
	012	2008 Aug 17 21:45	2008 Aug 18 02:50	54696.012	2237	187	187	187	375	462	751
	013	2008 Aug 24 07:45	2008 Aug 24 11:09	54702.394	2076	187	187	187	375	302	751
	014	2008 Aug 31 17:58	2008 Aug 31 23:04	54709.855	2598	206	214	214	428	518	857
	015	2008 Sep 7 10:45	2008 Sep 7 14:04	54716.517	2066	146	215	222	444	382	586
	016	2008 Sep 14 19:41	2008 Sep 14 21:32	54723.859	1755	151	151	151	303	345	606
	017	2008 Sep 21 15:37	2008 Sep 21 20:35	54730.754	2335	194	194	194	389	507	779
	018	2008 Sep 28 14:10	2008 Sep 28 16:04	54737.630	2085	176	176	176	352	439	704
	019	2008 Oct 5 07:02	2008 Oct 5 08:34	54744.325	1370	117	117	177	234	273	468
	020	2008 Oct 12 04:28	2008 Oct 12 07:53	54751.258	2464	202	202	202	405	559	810
	021	2008 Oct 19 16:29	2008 Oct 19 18:32	54758.729	2431	205	205	205	411	518	822
	022	2008 Oct 26 17:28	2008 Oct 26 20:50	54765.798	1802	117	187	187	375	215	641
	024	2008 Nov 5 16:29	2008 Nov 5 18:22	54775.726	1880	156	156	156	312	440	626
	025	2008 Nov 9 00:38	2008 Nov 9 02:34	54779.066	2267	186	186	186	372	535	744
	026	2008 Nov 16 01:25	2008 Nov 16 06:25	54786.163	2443	209	209	209	418	480	838
	028	2008 Nov 26 02:10	2008 Nov 26 05:32	54796.161	2078	172	173	173	346	434	692
	029	2008 Nov 30 01:04	2008 Nov 30 04:32	54800.114	1952	153	153	153	306	483	614
	030	2008 Dec 9 13:12	2008 Dec 9 15:08	54809.591	1947	160	160	160	322	442	645
	031	2008 Dec 16 04:10	2008 Dec 16 07:37	54816.246	2406	202	202	202	405	506	810
	033	2008 Dec 24 02:15	2008 Dec 24 12:02	54824.298	1951	160	160	160	320	404	641
	034	2008 Dec 28 16:34	2008 Dec 29 10:19	54829.060	3010	206	246	246	494	328	990
	035	2009 Jan 5 20:30	2009 Jan 5 24:00	54836.927	2002	168	168	168	336	429	673
	036	2009 Jan 11 05:09	2009 Jan 11 08:34	54842.286	2341	192	192	192	385	528	770
	037	2009 Jan 18 18:31	2009 Jan 18 22:02	54849.845	2641	212	212	212	425	638	850
	038	2009 Jan 25 11:15	2009 Jan 25 21:04	54856.673	1721	148	148	148	297	302	594
	039	2009 Feb 1 21:34	2009 Feb 2 04:01	54864.033	1130	23	132	132	265	...	492
	040	2009 May 23 08:21	2009 May 23 10:13	54974.387	1434	...	...	...	...	1419	...
	041	2009 May 30 20:17	2009 May 30 20:35	54981.852	1014	...	...	...	...	...	1007
	042	2009 Jun 3 01:13	2009 Jun 3 01:29	54985.051	933	...	...	...	...	...	931
	043	2009 Jun 7 00:03	2009 Jun 7 00:19	54989.008	858	...	...	...	...	...	1014
	045	2009 Jun 12 05:29	2009 Jun 12 05:46	54994.235	973	...	...	...	...	...	979

Table 1
(Continued)

ObsID	Segment	T-start[a]	T-stop[a]	MJD[b]	$T_{\rm XRT}$[c]	$T_{\rm V}$[3c]	$T_{\rm B}$[c]	$T_{\rm U}$[c]	$T_{\rm UVW1}$[c]	$T_{\rm UVM2}$[c]	$T_{\rm UVW2}$[c]
	046	2009 Jun 14 21:46	2009 Jun 14 23:35	54996.945	1505	...	...	...	...	...	1506
	047	2009 Jun 19 01:06	2009 Jun 19 02:52	55001.083	1843	...	...	...	...	...	1819
	048	2009 Jun 27 05:22	2009 Jun 27 07:06	55009.260	952	...	...	...	...	...	903
	049	2009 Jul 5 22:01	2009 Jul 5 22:20	55017.924	1090	...	...	...	...	...	1084
	050	2009 Jul 12 05:05	2009 Jul 12 05:22	55024.218	967	...	...	...	...	...	968
	051	2009 Jul 21 01:10	2009 Jul 21 01:28	55033.055	1049	...	...	...	...	...	1054
	052	2009 Jul 29 00:20	2009 Jul 29 03:48	55041.086	2099	...	...	...	...	...	2091
	053	2009 Aug 6 12:10	2009 Aug 6 14:08	55049.548	2236	...	...	...	...	...	2221
	054	2009 Aug 14 01:39	2009 Aug 14 03:34	55057.109	1291	...	...	...	...	...	1277
	055	2009 Aug 22 21:36	2009 Aug 22 23:44	55065.944	2063	...	...	...	...	...	2046
	056	2009 Aug 30 00:03	2009 Aug 30 05:06	55073.110	3243	...	...	...	...	...	3467
	057	2009 Sep 8 15:19	2009 Sep 8 18:42	55082.709	2218	...	...	...	...	...	2201
	058	2009 Sep 15 02:55	2009 Sep 15 04:45	55089.160	1893	...	...	...	...	...	1888
	059	2009 Sep 23 19:40	2009 Sep 23 23:05	55097.891	1959	...	...	...	...	...	1937
	060	2009 Oct 2 01:13	2009 Oct 1 03:07	55106.091	1930	...	...	...	...	...	1922
	061	2009 Oct 9 18:20	2009 Oct 9 20:13	55113.803	2109	...	...	...	...	...	2089
	062	2009 Oct 17 04:18	2009 Oct 17 06:10	55121.218	1899	161	161	161	323	396	645
	063	2009 Oct 25 23:05	2009 Oct 26 00:49	55129.998	565	...	86	86	313	...	73
	064	2009 Nov 2 02:35	2009 Nov 2 04:26	55137.146	1800	146	146	146	293	428	586
	065	2009 Nov 10 00:23	2009 Nov 10 02:03	55145.051	2108	95	210	210	421	279	837
	066	2009 Nov 18 10:43	2009 Nov 18 15:27	55153.545	2010	160	160	160	320	471	640
	067	2009 Nov 25 11:15	2009 Nov 25 13:07	55160.508	1949	161	161	161	322	429	645
	068	2009 Dec 4 21:40	2009 Dec 4 05:47	55170.072	2455	...	...	...	...	1735	690
	069	2009 Dec 11 23:56	2009 Dec 12 10:05	55177.208	1799	...	...	...	...	...	2044
	070	2009 Dec 20 00:41	2009 Dec 20 12:28	55185.274	2198	...	...	...	...	...	2186
	071	2009 Dec 28 01:25	2009 Dec 28 03:23	55193.100	2049	...	...	...	...	...	2038
	072	2010 Jan 5 21:32	2010 Jan 5 23:25	55201.937	1956	...	...	...	...	...	1949
	073	2010 Jan 13 00:01	2010 Jan 13 12:57	55209.270	2619	...	...	...	...	...	3036
	074	2010 Jan 25 21:41	2010 Jan 25 23:37	55221.944	2218	...	...	...	...	...	2200
	075	2010 Jan 29 22:08	2010 Jan 30 09:38	55226.162	2622	...	...	...	...	...	2596
	076	2010 Feb 6 03:36	2010 Feb 6 05:24	55233.188	1907	...	...	...	...	...	1914
35755	029	2010 May 21 02:12	2010 May 21 02:32	55337.098	1140	...	...	...	...	...	1149
	030	2010 Jun 14 08:59	2010 Jun 14 09:20	55361.382	1206	...	...	...	...	...	1203
	031	2010 Jul 16 01:01	2010 Jul 16 02:48	55393.080	1209	...	...	...	...	...	1209
	033	2010 Aug 10 12:57	2010 Aug 10 14:46	55418.577	1279	...	...	...	...	...	1279
	035	2010 Sep 14 16:03	2010 Sep 14 16:22	55453.676	1082	...	...	...	...	...	1082
	036	2010 Oct 4 09:43	2010 Oct 4 10:05	55473.413	1257	...	...	...	...	...	1251
	037	2010 Nov 1 21:53	2010 Nov 1 22:15	55501.920	1343	...	...	...	...	...	1339
	038	2010 Nov 29 01:34	2010 Nov 29 01:58	55529.074	1362	...	...	...	...	...	1361
	040	2010 Dec 31 15:46	2010 Dec 31 16:07	55561.665	1263	...	...	...	...	...	1266
	042	2011 Jan 24 22:43	2011 Jan 24 23:01	55585.953	1065	...	...	...	...	...	1049
	044	2011 May 20 18:12	2011 May 20 18:31	55701.765	1097	...	...	...	...	...	1102
	045	2011 Jun 17 01:31	2011 Jun 17 01:48	55729.069	977	...	...	...	...	...	983
	046	2011 Jul 15 23:05	2011 Jul 15 23:22	55757.968	982	...	...	...	...	...	987
	047	2011 Aug 12 15:48	2011 Aug 12 20:23	55785.754	1096	...	...	...	...	...	1088
	048	2011 Aug 14 22:15	2011 Aug 14 23:42	55787.957	1962	132	133	133	619	383	530
	049	2011 Aug 15 03:24	2011 Aug 15 06:22	55788.230	2943	...	...	...	...	...	2908
	050	2011 Aug 20 21-19	2011 Aug 20 21:34	55793.894	859	...	...	...	...	...	856
	051	2011 Aug 24 10:22	2011 Aug 24 13:44	55797.502	767	...	...	...	...	...	790
	052	2011 Aug 28 13:34	2011 Aug 28 13:50	55801.571	1006	...	...	...	...	...	1001
	053	2011 Sep 1 03:06	2011 Sep 1 22:14	55805.135	1094	...	...	...	...	...	1083
	054	2011 Sep 5 15:50	2011 Sep 5 16:08	55809.666	1025	...	...	...	...	...	1025
	055	2011 Sep 9 05:12	2011 Sep 9 15:10	55813.425	1058	...	...	...	...	...	1085
	056	2011 Sep 17 15.39	2011 Sep 17 15:52	55821.657	731	61	61	61	122	185	243
	057	2011 Sep 22 00:03	2011 Sep 22 06:37	55826.139	1140	...	...	...	...	...	1202
	058	2011 Sep 25 00:10	2011 Sep 25 00:26	55829.012	934	...	...	...	...	...	944
	059	2011 Sep 30 06:45	2011 Sep 30 07:05	55834.288	1145	...	...	...	...	...	1159
	060	2011 Oct 3 00:39	2011 Oct 3 00:59	55837.034	1215	...	...	...	...	...	1201
	061	2011 Oct 7 07:21	2011 Oct 7 07:37	55841.312	896	...	...	...	...	...	907
	062	2011 Oct 15 04:32	2011 Oct 15 06:36	55849.235	849	...	...	...	...	...	840
	063	2011 Oct 19 10:05	2011 Oct 19 10:20	55853.425	867	...	...	...	...	...	862
	064	2011 Oct 23 19:55	2011 Oct 23 20:04	55857.833	535	...	...	...	...	...	550
	065	2011 Oct 27 12:05	2011 Oct 27 12:24	55861.510	1015	...	...	...	...	...	1090
	066	2011 Oct 31 22:16	2011 Oct 31 22:33	55865.934	974	...	...	...	...	...	969
	067	2011 Nov 4 22:33	2011 Nov 4 22:50	55869.945	1016	...	...	...	...	...	1012
	068	2011 Nov 12 16:43	2011 Nov 12 17:00	55877.702	984	...	...	...	...	...	989

Table 1
(Continued)

ObsID	Segment	T-start[a]	T-stop[a]	MJD[b]	T_{XRT}[c]	T_V[3c]	T_B[c]	T_U[c]	T_{UVW1}[c]	T_{UVM2}[c]	T_{UVW2}[c]
	069	2011 Nov 16 13:42	2011 Nov 16 14:05	55881.579	1256	...	...	...	...	...	1328
	070	2011 Nov 20 15:17	2011 Nov 20 17:01	55885.673	1033	...	...	...	...	...	1029
	071	2011 Nov 24 19:07	2011 Nov 24 19:24	55889.802	1001	...	...	...	...	...	1011
	072	2011 Nov 28 11:24	2011 Nov 28 11:41	55893.481	989	...	...	...	...	...	977
	073	2011 Dec 2 03:18	2011 Dec 2 03:35	55897.144	989	...	...	...	...	...	984
	074	2011 Dec 6 13:26	2011 Dec 6 15:15	55901.598	1351	...	...	...	...	...	1336
	076	2011 Dec 14 02:45	2011 Dec 14 03:02	55909.121	976	...	...	...	...	...	973
	077	2011 Dec 18 02:56	2011 Dec 18 07:49	55913.224	807	...	...	...	...	...	812
	078	2011 Dec 23 00:03	2011 Dec 23 02:14	55918.048	1091	...	...	...	...	...	1310
	079	2011 Dec 26 11:45	2011 Dec 26 12:01	55921.495	939	...	...	...	...	...	945
	080	2011 Dec 30 11:51	2011 Dec 30 13:34	55925.530	1091	...	...	...	...	...	1076
	081	2012 Jan 3 12:30	2012 Jan 3 17:24	55929.623	1226	...	...	...	...	...	243
	082	2012 Jan 7 20:37	2012 Jan 7 20:54	55933.864	996	...	...	...	...	...	1002
	083	2012 Jan 11 04:53	2012 Jan 11 05:10	55937.209	999	...	...	...	...	...	999
	084	2012 Jan 12 07:45	2012 Jan 12 08:03	55938.329	1029	...	...	...	...	...	1033
	085	2012 Jan 13 03:03	2012 Jan 13 03:18	55939.132	844	...	...	...	...	...	852
	086	2012 Jan 14 01:28	2012 Jan 14 01:45	55940.067	969	...	...	...	...	...	973
	087	2012 Jan 15 04:45	2012 Jan 15 05:02	55941.204	976	...	...	...	...	...	985
	088	2012 Jan 16 03:12	2012 Jan 16 03:29	55942.139	976	...	...	...	...	...	973
	090	2012 Jan 18 22:43	2012 Jan 18 23:01	55944.953	1036	...	...	...	...	...	1042
	091	2012 Jan 19 19:28	2012 Jan 19 19:45	55945.817	967	...	...	...	...	...	974

Notes.
[a] Start and end times are given in UT.
[b] The MJD marks the middle of the observation.
[c] Observing time given in seconds.

Optical photometry was performed in five filters with the OM (Mason et al. 2001). The data are used to measure the optical-to-X-ray spectral energy distribution of Mkn 335 during the *XMM-Newton* observation. Due to slew problems at the beginning of the observations, V-filter observations were not obtained. All OM observations were performed in a science-user-defined configuration with a $7' \times 7'$ observing window.

The *XMM-Newton* data were processed in the standard way using the XMMSAS version *xmmsas_20100423_1803-10.0.0*. The EPIC pn data were checked for episodes of high particle background. At the end of the first orbit (ObsID 0600540601) the pn data were strongly affected by high particle background. Times with a background at energies $E > 10$ keV was larger than 10 counts s^{-1} were screened and not used for spectral analysis. This left an effective observing time of 99,036 s. During the second orbit (ObsID 0600540501) there were only very short episodes of high particle background. The total screened exposure time during this orbit was 69339 s.

The source X-ray photons in the EPIC pn and MOS were selected in a circular region with a radius of $1'$. Likewise, background photons were selected from a nearby, source-free region with the same radius. Only single and double events (`PATTERN.le.4`) and single to quadruple events (`PATTERN.le.12`) were selected for the pn and MOS data, respectively. The spectra were rebinned with the XMMSAS task *specgroup* with an oversampling of three of the resolution elements at the energy of the bin. The redistribution matrices and the auxiliary response files were created by the XMMSAS tasks *rmfgen* and *arfgen*, respectively. We included also the 2007 *XMM-Newton* pn data in our analysis. Note, however, that we also applied *specgroup* to rebin this spectrum and that the results may slightly differ from those presented in Grupe et al. (2008a). For comparison purposes, we also display the 2006 *XMM-Newton* high-state data in form of a light curve and hardness ratios.

RGS spectra and response matrices were created by the standard RGS XMMSAS tool *rgsproc*. The RGS spectra were rebinned with 10 photons bin^{-1} using *grppha*. Spectral fits to the EPIC pn and MOS, and RGS spectra were performed with XSPEC version 12.3.1x (Arnaud 1996). The OM data were processed with the XMMSAS task *omichain*. The magnitudes and fluxes of Mkn 335 were taken from the source lists created by the *omichain* task. For the count rate to flux conversion we used the conversion factors given in the OM Calibration document `XMM-SOC-CAL-TN-0019`.

2.3. Xinglong Optical Spectroscopy

The optical spectrum of Mkn 335 displays strong high-ionization iron coronal lines. In order to search for changes in the broad emission lines, and in the coronal lines, we have triggered an optical spectroscopic observation of Mkn 335 with the 2.16 m Xinglong telescope quasi-simultaneous with the 2009 *XMM-Newton* observation.

The data were acquired on 2009 July 31 with the Opto-Mechanics Research (OMR) spectrograph equipped with a 600 line mm^{-1} grating and the $2''$ slit. This setup produces a resolution of 5 Å. The spectrum of Mrk 335 was taken with 3600 s exposure.

Data reduction was done following standard procedures using IRAF. The CCD reductions included bias subtraction, flat-field correction, and cosmic-ray removal. Wavelength and flux calibration were performed.

We find that within the uncertainties there is no variability in the coronal lines, similar to our previous result (Grupe et al. 2008a).

3. RESULTS

3.1. Long-term Light Curve Observed by Swift

Figure 1 displays the *Swift* XRT count rate and hardness ratio light curves as well the UVOT light curves in each of the six

Table 2
XMM-Newton Observation Log of Mkn 335

Filter/Detector	*T*-start[a]	*T*-end[a]	*T*-exp[b]	Mag[c]	2007 Mag[d]
pn	2009 Jun 11 07:39	2009 Jun 12 19:54	114784		
MOS-1	2009 Jun 11 07:16	2009 Jun 12 19:57	131920		
MOS-2	2009 Jun 11 07:17	2009 Jun 12 19:57	131972		
pn	2009 Jun 13 07:31	2009 Jun 14 05:56	80344		
MOS-1	2009 Jun 13 07:08	2009 Jun 14 06:00	82257		
MOS-2	2009 Jun 13 07:08	2009 Jun 14 06:00	82249		
OM V	2009 Jun 11 07:25	2009 Jun 11 08:38	4400	14.47 ± 0.01	
OM U	2009 Jun 11 08:43	2009 Jun 11 09:57	4400	13.65 ± 0.01	13.36 ± 0.01
OM B	2009 Jun 11 10:02	2009 Jun 11 11:15	4400	14.73 ± 0.01	14.50 ± 0.01
OM W1	2009 Jun 11 11:20	2009 Jun 11 12:34	4400	13.34 ± 0.01	13.09 ± 0.01
OM W1	2009 Jun 11 12:39	2009 Jun 11 13:52	4400	13.34 ± 0.01	
OM W1	2009 Jun 11 14:26	2009 Jun 11 15:41	4400	13.34 ± 0.01	
OM M2	2009 Jun 11 15:46	2009 Jun 11 16:59	4400	13.37 ± 0.01	13.14 ± 0.01
OM M2	2009 Jun 11 17:04	2009 Jun 11 18:17	4400	13.39 ± 0.01	
OM M2	2009 Jun 11 18:22	2009 Jun 11 19:36	4400	13.40 ± 0.01	
ON M2	2009 Jun 11 20:59	2009 Jun 11 22:13	4400	13.21 ± 0.01	
OM W2	2009 Jun 11 22:18	2009 Jun 11 23:31	4400	13.48 ± 0.01	13.22 ± 0.01
OM W2	2009 Jun 11 23:36	2009 Jun 12 00:50	4400	13.48 ± 0.01	
OM W2	2009 Jun 12 00:55	2009 Jun 12 02:08	4400	13.49 ± 0.02	
OM W2	2009 Jun 12 02:13	2009 Jun 12 03:27	4400	13.48 ± 0.01	
OM W2	2009 Jun 12 03:32	2009 Jun 12 04:45	4400	13.47 ± 0.01	
OM W2	2009 Jun 12 04:50	2009 Jun 12 06:03	4400	13.48 ± 0.01	
OM W2	2009 Jun 12 06:09	2009 Jun 12 07:22	4400	13.48 ± 0.01	
OM W2	2009 Jun 12 07:27	2009 Jun 12 08:40	4400	13.48 ± 0.01	
OM W2	2009 Jun 12 08:45	2009 Jun 12 09:59	4400	13.48 ± 0.01	
OM W2	2009 Jun 12 10:34	2009 Jun 12 11:47	4400	13.48 ± 0.01	
OM W2	2009 Jun 12 11:52	2009 Jun 12 13:06	4400	13.46 ± 0.01	
OM W2	2009 Jun 12 13:11	2009 Jun 12 14:24	4400	13.48 ± 0.01	
OM W2	2009 Jun 12 14:29	2009 Jun 12 15:43	4400	13.46 ± 0.01	
OM W2	2009 Jun 12 15:48	2009 Jun 12 17:01	4400	13.48 ± 0.01	
OM W2	2009 Jun 12 17:06	2009 Jun 12 18:20	4400	13.45 ± 0.01	
OM W2	2009 Jun 12 18:25	2009 Jun 12 19:30	3920	13.47 ± 0.01	
OM V	2009 Jun 13 07:17	2009 Jun 13 08:30	4400	14.48 ± 0.01	
OM U	2009 Jun 13 08:35	2009 Jun 13 09:48	4400	13.67 ± 0.01	
OM B	2009 Jun 13 09:54	2009 Jun 13 11:07	4400	14.73 ± 0.01	
OM W1	2009 Jun 13 11:12	2009 Jun 13 12:25	4400	13.35 ± 0.01	
OM W1	2009 Jun 13 12:30	2009 Jun 13 13:44	4400	13.35 ± 0.01	
OM M2	2009 Jun 13 14:19	2009 Jun 13 15:32	4400	13.43 ± 0.01	
OM M2	2009 Jun 13 15:37	2009 Jun 13 16:50	4400	13.38 ± 0.01	
OM M2	2009 Jun 13 16:56	2009 Jun 13 18:09	4400	13.40 ± 0.01	
OM M2	2009 Jun 13 18:14	2009 Jun 13 19:28	4400	13.38 ± 0.01	
OM M2	2009 Jun 13 19:33	2009 Jun 13 20:46	4400	13.37 ± 0.01	
OM W2	2009 Jun 13 20:51	2009 Jun 13 22:41	4400	13:44 ± 0.01	
OM W2	2009 Jun 13 22:10	2009 Jun 13 23:23	4400	13:43 ± 0.01	
OM W2	2009 Jun 13 23:28	2009 Jun 14 00:42	4400	13:44 ± 0.01	
OM W2	2009 Jun 14 00:47	2009 Jun 14 02:00	4400	13:46 ± 0.01	
OM W2	2009 Jun 14 02:05	2009 Jun 14 03:18	4400	13:46 ± 0.01	
OM W2	2009 Jun 14 03:23	2009 Jun 14 04:37	4400	13:47 ± 0.01	
OM W2	2009 Jun 14 04:42	2009 Jun 14 05:33	3100	13:46 ± 0.01	

Notes.
[a] Start and end times are given in UT.
[b] Exposure times given in seconds.
[c] Observed magnitudes not corrected for Galactic reddening at the position of Mkn 335.
[d] The 2007 OM data are listed here as a comparison to the 2009 observations. For the exact observing time we refer to Grupe et al. (2008a).

filters. Note that after the end of the *Swift* GI program for Mkn 335 in 2009 January, we limited the UVOT observations to W2 in order to reduce the UVOT filter wheel rotations. The vertical lines in Figure 1 mark the times of the 2007 and 2009 *XMM-Newton* observations. The XRT count rates, hardness ratios, and UVOT magnitudes for these light curves are summarized in Table 3. Note that the 2009 *XMM-Newton* observation was performed from MJD 54993.3188 to 54996.2500. Compared with the time at which we triggered the 2009 *XMM-Newton* observation, Mkn 335 had become significantly brighter and we found Mkn 335 in an interesting transition into an intermediate-flux state. It increased its average XRT count rate from about 0.11 to 0.36 counts s^{-1} during the time of the *XMM-Newton* observation. The left panel in

Table 3
Swift XRT Count Rates and Hardness Ratios and UVOT Magnitudes[a] of Mkn 335

ObsID	Segment	MJD	XRT CR	XRT HR	V	B	U	UVW1	UVM2	UVW2
35755	001	54237.128	0.053 ± 0.004	+0.07 ± 0.03	14.22 ± 0.01	14.49 ± 0.01	13.29 ± 0.01	13.20 ± 0.01	13.12 ± 0.01	13.19 ± 0.01
	002	54245.406	0.144 ± 0.004	+0.06 ± 0.03	14.19 ± 0.01	14.42 ± 0.01	13.20 ± 0.01	13.08 ± 0.01	12.95 ± 0.01	13.01 ± 0.01
	003	54279.073	0.076 ± 0.012	+0.10 ± 0.07	14.19 ± 0.01	14.44 ± 0.01	13.23 ± 0.01	13.09 ± 0.01	12.98 ± 0.01	13.04 ± 0.01
	004	54281.314	0.082 ± 0.006	+0.04 ± 0.07	14.15 ± 0.01	14.41 ± 0.01	13.22 ± 0.01	13.10 ± 0.01	12.97 ± 0.01	13.04 ± 0.01
	005	54283.751	0.109 ± 0.007	−0.15 ± 0.06	14.18 ± 0.01	14.42 ± 0.01	13.23 ± 0.01	13.05 ± 0.01	12.93 ± 0.01	12.98 ± 0.01
	008	54362.219	0.420 ± 0.020	−0.15 ± 0.05	...	...	...	...	...	...
	009	54368.141	0.634 ± 0.021	−0.07 ± 0.03	...	...	...	...	...	...
	010	54377.068	0.154 ± 0.011	+0.25 ± 0.07	...	...	...	...	...	...
	011	54380.795	0.324 ± 0.011	−0.05 ± 0.03	...	...	...	...	...	...
	012	54381.799	0.137 ± 0.007	+0.05 ± 0.05	...	...	...	...	...	...
	013	54382.569	0.380 ± 0.010	−0.01 ± 0.03	...	...	...	...	...	...
	014	54383.569	0.232 ± 0.009	+0.03 ± 0.04	...	...	...	...	...	...
	015	54384.514	0.451 ± 0.013	−0.12 ± 0.03	...	...	...	...	...	...
	016	54386.084	0.494 ± 0.009	+0.01 ± 0.02	...	...	...	...	...	...
	017	54390.198	0.885 ± 0.025	−0.01 ± 0.02	...	...	...	...	...	...
	018	54391.327	1.277 ± 0.020	−0.01 ± 0.05	...	...	...	...	...	...
	019	54393.000	0.881 ± 0.020	−0.03 ± 0.01	...	...	...	...	...	...
	020	54394.899	1.109 ± 0.025	−0.07 ± 0.02	...	...	...	...	...	...
	021	54404.766	0.978 ± 0.032	−0.12 ± 0.03	14.16 ± 0.02	14.38 ± 0.01	13.20 ± 0.01	13.01 ± 0.01	12.93 ± 0.01	12.93 ± 0.01
	022	54439.194	0.754 ± 0.015	−0.03 ± 0.02	14.10 ± 0.01	14.35 ± 0.01	13.10 ± 0.01	12.93 ± 0.01	12.79 ± 0.01	12.81 ± 0.01
	023	54446.536	0.652 ± 0.023	−0.03 ± 0.03	14.12 ± 0.02	14.31 ± 0.01	13.11 ± 0.01	12.94 ± 0.01	12.77 ± 0.01	12.81 ± 0.01
	024	54453.890	0.298 ± 0.013	−0.05 ± 0.05	14.14 ± 0.02	14.35 ± 0.01	13.14 ± 0.01	12.98 ± 0.01	12.87 ± 0.01	12.92 ± 0.01
	025	54460.586	0.253 ± 0.012	−0.06 ± 0.05	14.19 ± 0.02	14.40 ± 0.01	13.15 ± 0.01	13.02 ± 0.01	12.90 ± 0.01	12.94 ± 0.01
	026	54467.404	0.925 ± 0.024	−0.10 ± 0.02	14.16 ± 0.01	14.39 ± 0.01	13.19 ± 0.01	13.01 ± 0.01	12.87 ± 0.01	12.91 ± 0.01
	027	54474.935	0.534 ± 0.018	−0.01 ± 0.03	14.13 ± 0.01	14.37 ± 0.01	13.18 ± 0.01	13.10 ± 0.01	12.88 ± 0.01	12.92 ± 0.01
90006	001	54618.619	0.503 ± 0.026	+0.01 ± 0.03	14.33 ± 0.02	14.46 ± 0.01	13.27 ± 0.01	13.11 ± 0.01	13.00 ± 0.01	13.05 ± 0.01
	002	54625.095	0.892 ± 0.028	−0.10 ± 0.02	14.20 ± 0.02	14.48 ± 0.01	13.24 ± 0.01	13.06 ± 0.01	12.93 ± 0.01	12.97 ± 0.01
	003	54632.074	1.058 ± 0.033	+0.02 ± 0.02	14.20 ± 0.01	14.45 ± 0.01	13.27 ± 0.01	13.11 ± 0.01	12.97 ± 0.01	13.01 ± 0.01
	004	54639.484	1.121 ± 0.015	−0.06 ± 0.01	14.21 ± 0.01	14.44 ± 0.01	13.23 ± 0.01	13.06 ± 0.01	12.92 ± 0.01	12.96 ± 0.01
	005	54646.645	0.382 ± 0.013	−0.08 ± 0.03	14.26 ± 0.02	14.45 ± 0.01	13.25 ± 0.01	13.11 ± 0.01	12.97 ± 0.01	13.03 ± 0.01
	006	54653.030	0.800 ± 0.025	−0.00 ± 0.03	14.18 ± 0.02	14.43 ± 0.01	13.21 ± 0.01	13.03 ± 0.01	12.89 ± 0.01	12.93 ± 0.01
	007	54660.909	1.093 ± 0.040	−0.04 ± 0.03	14.22 ± 0.02	14.44 ± 0.01	13.25 ± 0.01	13.07 ± 0.01	12.91 ± 0.01	12.94 ± 0.01
	008	54667.165	1.000 ± 0.043	−0.04 ± 0.03	14.23 ± 0.03	14.43 ± 0.01	13.25 ± 0.01	13.06 ± 0.01	12.95 ± 0.02	12.99 ± 0.01
	009	54674.390	1.206 ± 0.034	−0.09 ± 0.03	14.22 ± 0.02	14.47 ± 0.01	13.26 ± 0.01	13.09 ± 0.01	12.95 ± 0.01	12.98 ± 0.01
	010	54681.542	1.078 ± 0.028	+0.04 ± 0.02	14.16 ± 0.02	14.40 ± 0.01	13.16 ± 0.01	13.00 ± 0.01	12.83 ± 0.01	12.87 ± 0.01
	011	54688.615	1.138 ± 0.030	−0.11 ± 0.02	14.17 ± 0.02	14.42 ± 0.01	13.19 ± 0.01	13.04 ± 0.01	12.91 ± 0.01	12.92 ± 0.01
	012	54696.012	0.781 ± 0.025	−0.03 ± 0.03	14.21 ± 0.01	14.45 ± 0.01	13.26 ± 0.01	13.12 ± 0.01	12.99 ± 0.01	13.04 ± 0.01
	013	54702.394	1.315 ± 0.037	+0.01 ± 0.03	14.21 ± 0.01	14.44 ± 0.01	13.27 ± 0.01	13.03 ± 0.01	13.05 ± 0.01	13.04 ± 0.01
	014	54709.855	0.502 ± 0.017	+0.02 ± 0.03	14.31 ± 0.01	14.56 ± 0.01	13.41 ± 0.01	13.31 ± 0.01	13.24 ± 0.01	13.31 ± 0.01
	015	54716.517	0.348 ± 0.014	+0.02 ± 0.04	14.33 ± 0.02	14.57 ± 0.01	13.39 ± 0.01	13.27 ± 0.01	13.18 ± 0.01	13.24 ± 0.01
	016	54723.859	0.532 ± 0.019	−0.04 ± 0.03	14.24 ± 0.02	14.50 ± 0.01	13.33 ± 0.01	13.19 ± 0.01	13.08 ± 0.01	13.12 ± 0.01
	017	54730.754	0.809 ± 0.027	−0.06 ± 0.03	14.28 ± 0.02	14.51 ± 0.01	13.32 ± 0.01	13.19 ± 0.01	13.06 ± 0.01	13.12 ± 0.01
	018	54737.630	0.605 ± 0.024	+0.02 ± 0.03	14.24 ± 0.02	14.53 ± 0.01	13.37 ± 0.01	13.27 ± 0.01	13.15 ± 0.01	13.22 ± 0.01
	019	54744.325	0.907 ± 0.032	−0.04 ± 0.03	14.29 ± 0.02	14.58 ± 0.01	13.36 ± 0.01	13.26 ± 0.01	13.12 ± 0.01	13.18 ± 0.01
	020	54751.258	0.493 ± 0.015	+0.02 ± 0.03	14.29 ± 0.01	14.55 ± 0.01	13.39 ± 0.01	13.23 ± 0.01	13.11 ± 0.01	13.18 ± 0.01
	021	54758.729	0.758 ± 0.023	−0.14 ± 0.03	14.34 ± 0.02	14.54 ± 0.01	13.40 ± 0.01	13.23 ± 0.01	13.10 ± 0.01	13.15 ± 0.01
	022	54765.798	0.514 ± 0.018	−0.02 ± 0.03	14.22 ± 0.02	14.48 ± 0.01	13.30 ± 0.01	13.23 ± 0.01	12.98 ± 0.01	13.07 ± 0.01
	024	54775.726	1.041 ± 0.029	−0.06 ± 0.03	14.20 ± 0.02	14.46 ± 0.01	13.29 ± 0.01	13.07 ± 0.01	12.96 ± 0.01	13.01 ± 0.01
	025	54779.066	1.141 ± 0.028	−0.09 ± 0.02	14.19 ± 0.01	14.46 ± 0.01	13.29 ± 0.01	13.08 ± 0.01	12.97 ± 0.01	13.07 ± 0.01
	026	54786.163	1.042 ± 0.026	−0.06 ± 0.02	14.20 ± 0.01	14.44 ± 0.01	13.23 ± 0.01	13.08 ± 0.01	12.94 ± 0.01	13.01 ± 0.01
	028	54796.161	0.474 ± 0.017	−0.00 ± 0.03	14.18 ± 0.02	14.46 ± 0.01	13.29 ± 0.01	13.10 ± 0.01	12.97 ± 0.01	13.04 ± 0.01
	029	54800.114	1.110 ± 0.031	−0.08 ± 0.03	14.25 ± 0.02	14.44 ± 0.01	13.25 ± 0.01	13.07 ± 0.01	12.93 ± 0.01	12.98 ± 0.01
	030	54809.591	0.868 ± 0.027	−0.01 ± 0.03	14.29 ± 0.02	14.44 ± 0.01	13.24 ± 0.01	13.07 ± 0.01	12.94 ± 0.01	12.99 ± 0.01
	031	54816.246	0.432 ± 0.018	+0.01 ± 0.04	14.26 ± 0.01	14.51 ± 0.01	13.35 ± 0.01	13.13 ± 0.01	13.04 ± 0.01	13.10 ± 0.01
	033	54824.298	0.925 ± 0.029	−0.05 ± 0.03	14.24 ± 0.02	14.48 ± 0.01	13.26 ± 0.01	13.08 ± 0.01	12.93 ± 0.01	12.98 ± 0.01
	034	54829.060	0.863 ± 0.022	+0.02 ± 0.02	14.25 ± 0.01	14.50 ± 0.01	13.29 ± 0.01	13.12 ± 0.01	12.98 ± 0.01	13.04 ± 0.01
	035	54836.927	0.689 ± 0.024	+0.03 ± 0.03	14.23 ± 0.02	14.51 ± 0.01	13.30 ± 0.01	13.13 ± 0.01	12.98 ± 0.01	13.04 ± 0.01
	036	54842.286	1.521 ± 0.040	−0.02 ± 0.02	14.19 ± 0.01	14.44 ± 0.01	13.22 ± 0.01	13.05 ± 0.01	12.88 ± 0.01	12.92 ± 0.01
	037	54849.845	1.543 ± 0.047	−0.05 ± 0.02	14.22 ± 0.01	14.44 ± 0.01	13.23 ± 0.01	13.03 ± 0.01	12.86 ± 0.01	12.88 ± 0.01
	038	54856.673	0.389 ± 0.017	−0.03 ± 0.04	14.19 ± 0.02	14.45 ± 0.01	13.22 ± 0.01	13.06 ± 0.01	12.92 ± 0.01	12.98 ± 0.01
	039	54864.033	0.860 ± 0.034	+0.03 ± 0.03	14.14 ± 0.04	14.51 ± 0.01	13.22 ± 0.01	13.11 ± 0.01	...	13.05 ± 0.01
	040	54974.387	0.434 ± 0.025	+0.01 ± 0.05	...	...	...	...	13.06 ± 0.01	...
	041	54981.852	0.171 ± 0.015	+0.11 ± 0.09	...	...	...	...	...	13.24 ± 0.01
	042	54985.051	0.111 ± 0.011	+0.13 ± 0.09	...	...	...	...	...	13.28 ± 0.01
	043	54989.008	0.125 ± 0.013	+0.08 ± 0.10	...	...	...	...	...	13.25 ± 0.01
	045	54994.235	0.171 ± 0.015	+0.02 ± 0.09	...	...	...	...	...	13.28 ± 0.01

Table 3
(Continued)

ObsID	Segment	MJD	XRT CR	XRT HR	V	B	U	UVW1	UVM2	UVW2
	046	54996.945	0.361 ± 0.016	+0.09 ± 0.05	...	...	...	...	...	13.22 ± 0.01
	047	55001.083	0.303 ± 0.014	+0.03 ± 0.05	...	...	...	...	...	13.10 ± 0.01
	048	55009.260	0.362 ± 0.021	+0.10 ± 0.06	...	...	...	...	...	13.26 ± 0.01
	049	55017.924	0.552 ± 0.027	+0.01 ± 0.04	...	...	...	...	...	13.20 ± 0.01
	050	55024.218	0.412 ± 0.022	+0.12 ± 0.05	...	...	...	...	...	13.19 ± 0.01
	051	55033.055	0.225 ± 0.025	+0.04 ± 0.10	...	...	...	...	...	13.19 ± 0.01
	052	55041.086	0.180 ± 0.010	+0.13 ± 0.05	...	...	...	...	...	13.14 ± 0.01
	053	55049.548	0.123 ± 0.008	+0.17 ± 0.06	...	...	...	...	...	13.24 ± 0.01
	054	55057.109	0.098 ± 0.009	+0.12 ± 0.09	...	...	...	...	...	13.19 ± 0.01
	055	55065.944	0.197 ± 0.012	+0.09 ± 0.05	...	...	...	...	...	13.04 ± 0.01
	056	55073.110	0.155 ± 0.008	+0.06 ± 0.05	...	...	...	...	...	13.12 ± 0.01
	057	55082.709	0.203 ± 0.010	+0.20 ± 0.05	...	...	...	...	...	12.99 ± 0.01
	058	55089.160	0.392 ± 0.019	−0.10 ± 0.05	...	...	...	...	...	12.90 ± 0.01
	059	55097.891	0.052 ± 0.019	−0.06 ± 0.04	...	...	...	...	...	12.92 ± 0.01
	060	55106.091	0.130 ± 0.010	+0.23 ± 0.07	...	...	...	...	...	13.05 ± 0.01
	061	55113.803	0.118 ± 0.008	+0.34 ± 0.06	...	...	...	...	...	13.14 ± 0.01
	062	55121.218	0.082 ± 0.009	+0.26 ± 0.10	14.33 ± 0.02	14.55 ± 0.01	13.34 ± 0.01	13.25 ± 0.01	13.15 ± 0.01	13.22 ± 0.01
	063	55129.998	0.144 ± 0.017	+0.07 ± 0.11	...	14.47 ± 0.01	13.29 ± 0.01	13.10 ± 0.01	...	13.10 ± 0.01
	064	55137.146	0.133 ± 0.009	+0.22 ± 0.07	14.25 ± 0.02	14.51 ± 0.01	13.26 ± 0.01	13.15 ± 0.01	13.04 ± 0.01	13.08 ± 0.01
	065	55145.051	0.076 ± 0.007	+0.09 ± 0.08	14.20 ± 0.02	14.47 ± 0.01	13.27 ± 0.01	13.08 ± 0.01	12.98 ± 0.01	13.04 ± 0.01
	066	55153.545	0.105 ± 0.008	+0.29 ± 0.07	14.30 ± 0.02	14.51 ± 0.01	13.30 ± 0.01	13.12 ± 0.01	13.01 ± 0.01	13.04 ± 0.01
	067	55160.508	0.438 ± 0.017	−0.03 ± 0.04	14.18 ± 0.02	14.42 ± 0.01	13.17 ± 0.01	12.99 ± 0.01	12.82 ± 0.01	12.85 ± 0.01
	068	55170.072	0.082 ± 0.006	+0.18 ± 0.07	...	...	...	...	12.83 ± 0.01	12.97 ± 0.01
	069	55177.208	0.143 ± 0.010	+0.11 ± 0.07	...	...	...	...	...	12.97 ± 0.01
	070	55185.274	0.189 ± 0.014	+0.12 ± 0.07	...	...	...	...	...	12.93 ± 0.01
	071	55193.100	0.121 ± 0.010	+0.20 ± 0.07	...	...	...	...	...	13.05 ± 0.01
	072	55201.937	0.291 ± 0.015	+0.05 ± 0.05	...	...	...	...	...	13.07 ± 0.01
	073	55209.270	0.477 ± 0.015	+0.06 ± 0.03	...	...	...	...	...	13.21 ± 0.01
	074	55221.944	0.232 ± 0.011	+0.08 ± 0.05	...	...	...	...	...	13.31 ± 0.01
	075	55226.162	0.436 ± 0.014	−0.01 ± 0.03	...	...	...	...	...	13.26 ± 0.01
	076	55233.188	0.512 ± 0.021	−0.02 ± 0.04	...	...	...	...	...	13.16 ± 0.01
35755	029	55337.098	0.121 ± 0.011	+0.05 ± 0.09	...	...	...	...	...	13.14 ± 0.01
	030	55361.381	0.158 ± 0.012	+0.19 ± 0.08	...	...	...	...	...	13.19 ± 0.01
	031	55393.080	0.402 ± 0.020	+0.05 ± 0.05	...	...	...	...	...	13.29 ± 0.01
	033	55418.577	0.186 ± 0.013	+0.15 ± 0.07	...	...	...	...	...	13.25 ± 0.01
	035	55453.676	0.228 ± 0.016	+0.11 ± 0.07	...	...	...	...	...	13.53 ± 0.01
	036	55473.413	0.330 ± 0.018	−0.02 ± 0.05	...	...	...	...	...	13.23 ± 0.01
	037	55501.920	0.734 ± 0.028	−0.15 ± 0.03	...	...	...	...	...	13.07 ± 0.01
	038	55529.074	0.135 ± 0.011	+0.15 ± 0.08	...	...	...	...	...	12.94 ± 0.01
	040	55561.665	0.478 ± 0.021	−0.16 ± 0.04	...	...	...	...	...	12.74 ± 0.01
	042	55585.953	0.140 ± 0.012	+0.04 ± 0.09	...	...	...	...	...	12.91 ± 0.01
	044	55701.765	0.085 ± 0.010	+0.01 ± 0.10	...	...	...	...	...	12.92 ± 0.01
	045	55729.069	0.191 ± 0.015	−0.02 ± 0.08	...	...	...	...	...	12.69 ± 0.01
	046	55757.968	0.094 ± 0.010	+0.18 ± 0.11	...	...	...	...	...	13.03 ± 0.01
	047	55785.754	0.058 ± 0.008	−0.12 ± 0.13	...	...	...	...	...	13.03 ± 0.01
	048	55787.957	0.084 ± 0.008	+0.08 ± 0.09	14.32 ± 0.02	14.51 ± 0.01	13.31 ± 0.01	13.17 ± 0.01	13.03 ± 0.01	13.05 ± 0.01
	049	55788.203	0.095 ± 0.006	−0.09 ± 0.06	...	...	...	...	...	13.07 ± 0.01
	050	55793.894	0.128 ± 0.014	+0.13 ± 0.11	...	...	...	...	...	13.09 ± 0.01
	051	55797.502	0.066 ± 0.010	+0.32 ± 0.15	...	...	...	...	...	13.14 ± 0.01
	052	55801.571	0.042 ± 0.010	−0.19 ± 0.20	...	...	...	...	...	13.20 ± 0.01
	053	55805.135	0.062 ± 0.010	+0.27 ± 0.13	...	...	...	...	...	13.18 ± 0.01
	054	55809.666	0.098 ± 0.011	+0.33 ± 0.11	...	...	...	...	...	13.26 ± 0.01
	055	55813.425	0.067 ± 0.009	−0.23 ± 0.13	...	...	...	...	...	13.63 ± 0.01
	056	55821.657	0.076 ± 0.011	+0.12 ± 0.14	14.38 ± 0.03	14.61 ± 0.02	13.42 ± 0.01	13.34 ± 0.01	13.19 ± 0.02	13.26 ± 0.01
	057	55826.139	0.083 ± 0.009	+0.01 ± 0.11	...	...	...	...	...	13.21 ± 0.01
	058	55829.012	0.194 ± 0.015	+0.06 ± 0.08	...	...	...	...	...	13.21 ± 0.01
	059	55834.288	0.079 ± 0.009	+0.09 ± 0.11	...	...	...	...	...	13.24 ± 0.01
	060	55837.034	0.081 ± 0.009	+0.27 ± 0.10	...	...	...	...	...	13.21 ± 0.01
	061	55841.312	0.057 ± 0.011	−0.14 ± 0.18	...	...	...	...	...	13.24 ± 0.01
	062	55849.235	0.052 ± 0.013	+0.07 ± 0.21	...	...	...	...	...	13.16 ± 0.01
	063	55853.425	0.058 ± 0.009	−0.22 ± 0.15	...	...	...	...	...	13.04 ± 0.03
	064	55857.833	0.099 ± 0.015	+0.07 ± 0.14	...	...	...	...	...	12.99 ± 0.01
	065	55861.510	0.134 ± 0.012	+0.19 ± 0.09	...	...	...	...	...	13.01 ± 0.01
	066	55865.934	0.460 ± 0.025	−0.13 ± 0.05	...	...	...	...	...	13.09 ± 0.03
	067	55869.945	0.321 ± 0.019	−0.10 ± 0.06	...	...	...	...	...	12.91 ± 0.01
	068	55877.702	0.132 ± 0.012	−0.01 ± 0.09	...	...	...	...	...	12.89 ± 0.02

Table 3
(Continued)

ObsID	Segment	MJD	XRT CR	XRT HR	V	B	U	UVW1	UVM2	UVW2
	069	55881.578	0.436 ± 0.019	−0.07 ± 0.05	. . .	. . .	. . .	. . .	. . .	12.90 ± 0.02
	070	55885.673	0.961 ± 0.038	−0.05 ± 0.03	. . .	. . .	. . .	. . .	. . .	12.89 ± 0.02
	071	55889.802	0.347 ± 0.020	−0.04 ± 0.06	. . .	. . .	. . .	. . .	. . .	12.88 ± 0.02
	072	55893.481	0.493 ± 0.024	−0.13 ± 0.05	. . .	. . .	. . .	. . .	. . .	12.96 ± 0.02
	073	55897.144	0.555 ± 0.026	−0.00 ± 0.04	. . .	. . .	. . .	. . .	. . .	12.93 ± 0.02
	074	55901.598	0.595 ± 0.025	−0.09 ± 0.06	. . .	. . .	. . .	. . .	. . .	12.99 ± 0.02
	076	55909.121	0.192 ± 0.015	−0.17 ± 0.07	. . .	. . .	. . .	. . .	. . .	13.24 ± 0.02
	077	55913.224	0.207 ± 0.020	−0.17 ± 0.09	. . .	. . .	. . .	. . .	. . .	13.06 ± 0.03
	078	55918.048	0.130 ± 0.013	−0.10 ± 0.10	. . .	. . .	. . .	. . .	. . .	13.07 ± 0.03
	079	55921.495	0.797 ± 0.036	−0.16 ± 0.04	. . .	. . .	. . .	. . .	. . .	12.93 ± 0.03
	080	55925.530	0.301 ± 0.018	+0.07 ± 0.06	. . .	. . .	. . .	. . .	. . .	12.86 ± 0.03
	081	55929.623	1.283 ± 0.047	−0.06 ± 0.05	. . .	. . .	. . .	. . .	. . .	12.89 ± 0.03
	082	55933.864	0.477 ± 0.024	−0.17 ± 0.06	. . .	. . .	. . .	. . .	. . .	12.91 ± 0.03
	083	55937.209	0.692 ± 0.033	−0.14 ± 0.06	. . .	. . .	. . .	. . .	. . .	12.78 ± 0.03
	084	55938.329	0.344 ± 0.020	−0.05 ± 0.06	. . .	. . .	. . .	. . .	. . .	12.77 ± 0.03
	085	55939.132	0.306 ± 0.025	−0.14 ± 0.08	. . .	. . .	. . .	. . .	. . .	12.79 ± 0.03
	086	55940.067	0.283 ± 0.018	−0.21 ± 0.06	. . .	. . .	. . .	. . .	. . .	12.78 ± 0.03
	087	55941.204	0.373 ± 0.021	−0.18 ± 0.05	. . .	. . .	. . .	. . .	. . .	12.77 ± 0.03
	088	55942.139	1.024 ± 0.040	−0.20 ± 0.05	. . .	. . .	. . .	. . .	. . .	12.74 ± 0.03
	090	55944.953	0.690 ± 0.032	−0.18 ± 0.05	. . .	. . .	. . .	. . .	. . .	12.67 ± 0.03
	091	55945.817	1.213 ± 0.044	−0.11 ± 0.05	. . .	. . .	. . .	. . .	. . .	12.70 ± 0.03

Note. [a] Magnitude corrected for reddening with $E_{B-V} = 0.037$ given by Schlegel et al. (1998). The errors given in this table are statistical errors.

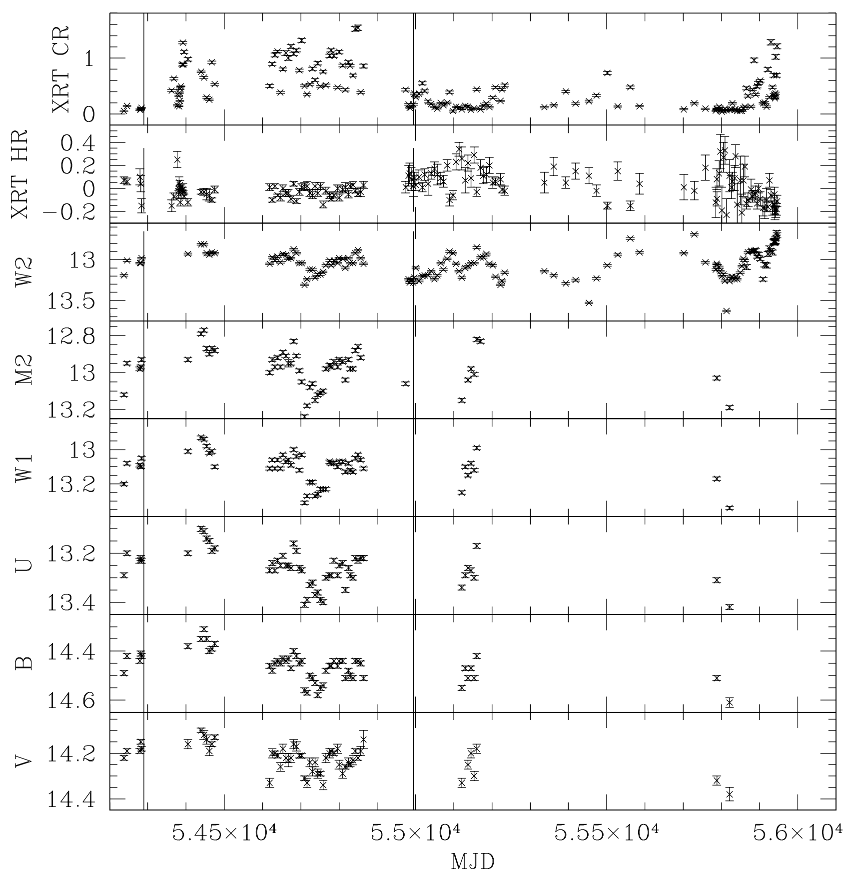

Figure 1. *Swift* XRT and UVOT light curves of Mkn 335. The vertical lines at MJD 54290 and 54995 mark the times of the *XMM-Newton* observations in 2007 July and 2009 June. The beginning of the light curve is 2007 May 17.

Figure 2 displays the *Swift* XRT and UVOT W2 light curves before and after the 2009 *XMM-Newton* observation.

When we started monitoring Mkn 335 in 2007 May, it was in its historical low state as we reported in Grupe et al. (2007a). However, it became significantly brighter starting from 2007 September and Mkn 335 remained in this intermediate state throughout 2008 (Figure 1). Due to a failure of one of the *Swift* gyros (Grupe et al. 2007a) the UVOT was turned off in 2007

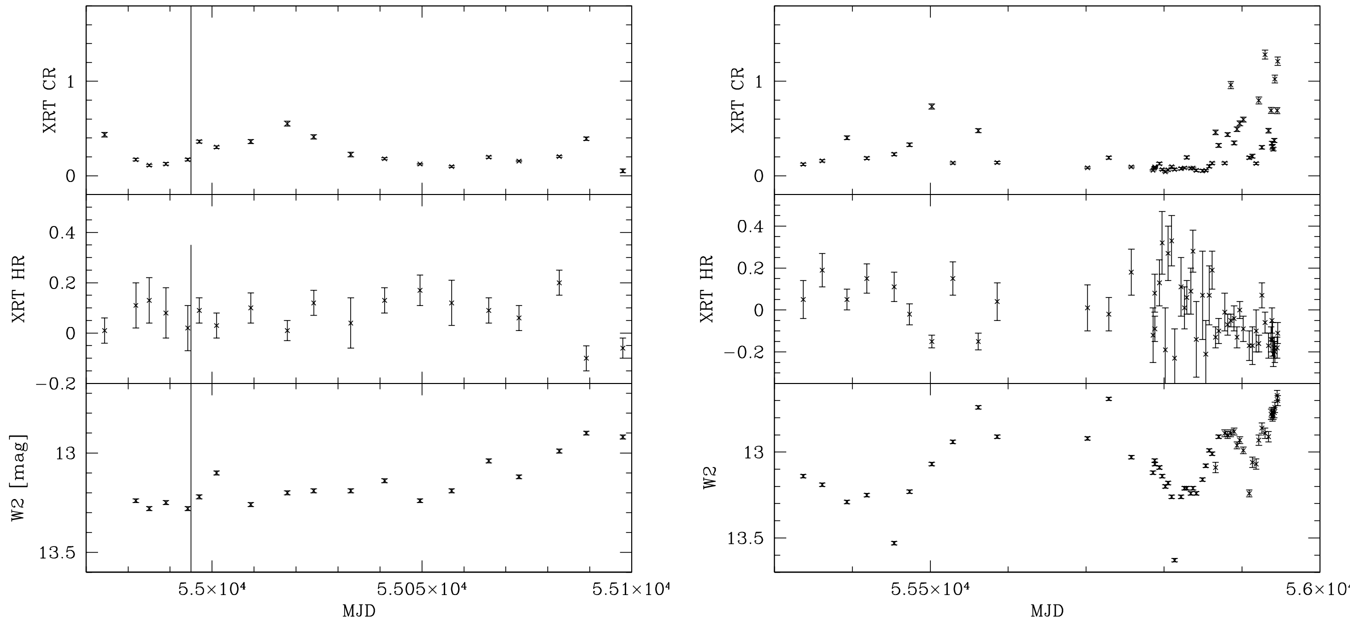

Figure 2. Zoom-in of the *Swift* XRT and UVOT W2 light curves of Mkn 335. The left panel displays the *Swift* observations before and shortly after the 2009 *XMM-Newton* observation. The vertical line at MJD 54995 marks the time of the *XMM-Newton* observation in 2009 June. The beginning of this light curve is 2009 May 23. The right panel shows the light curves in 2010 and 2011.

September and October. When we started monitoring Mkn 335 again after it came out of the *Swift* Sun constraint in 2009 May, we found Mkn 335 back in a low state. This low state was the reason why we triggered our pre-approved *XMM-Newton* observation. Mkn 335 remained in a low state throughout 2009 with a slight increase toward the end of that monitoring episode. In 2010 Mkn 335 has been in a low state for most of the time. After emerging from the *Swift* Sun constraint in 2011 May, it shows again a very low state with a *Swift* XRT count rate of 0.08 counts s^{-1} and even displayed an all-time low state on 2011 August 28 with a count rate of 0.042 ± 0.010 counts s^{-1} (right panel in Figure 2). However, recently in 2011 November Mkn 335 went into a high-state peaking at about 1 count s^{-1} in the XRT. We therefore changed our observing strategy to a four-day cadence. Mkn 335 is now showing a very rapid variability behavior suggesting that it switches into a high state. Currently (2012 January), we are observing Mkn 335 daily. On 2012 January 11, it displayed the highest XRT count rate measured since 2009 January with 1.3 counts s^{-1}. This X-ray flux is comparable to the 2006 *XMM-Newton* observation shown in Figure 6.

One question regarding a highly variable source like Mkn 335 is, does the spectral shape change with X-ray flux? As we have shown already in Grupe et al. (2008a) the X-ray spectra of Mkn 335 look completely different in the low and high states. The low number of photons in the *Swift* XRT spectra, however, does not allow us to perform a detailed spectral analysis. Still, a hardness ratio provides some clues about the changes in the X-ray spectrum. Figure 3 shows the relation between the count rate and hardness ratio in the *Swift* data.[11] Figure 3 suggests that the AGN becomes softer with increasing count rate. This results is a linear correlation coefficient $r_l = -0.580$ and a Spearman rank order correlation coefficient $r_s = -0.69$ with a Student's T-value $T_s = -9.4$. For both correlations the probability of a random results is $P < 10^{-6}$.

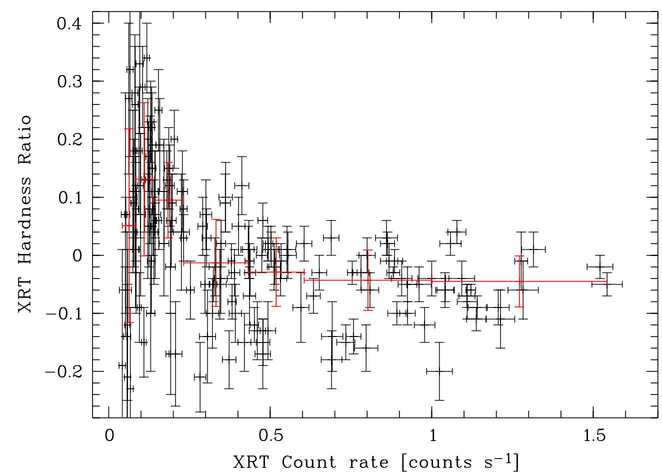

Figure 3. Count rate vs. hardness ratio during the *Swift* observations. The red crosses correspond to bins in count rate containing 25 measurements and the mean hardness ratio and standard deviation in that bin.

(A color version of this figure is available in the online journal.)

As shown in Figure 1, Mkn 335 also shows variability in all six UVOT filters. During the 2009 *XMM-Newton* observation, Mkn 335 appeared to be slightly fainter by about 0.2–0.3 mag in the OM B, U, W1, M2, and W2 filters (Table 2) compared with the 2007 observation. This is in agreement with the *Swift* UVOT light curves displayed in Figure 1. As listed in Table 3, in the UVOT W2 filter Mkn 335 was about 0.3 mag brighter during the 2007 May X-ray low state compared with the 2009 May/June low state. UV variability by 0.3 mag is quite common among NLS1s (Grupe et al. 2010). However, Mkn 335 exhibited a remarkable change in W2 in 2010 as displayed in the right panel of Figure 2 when after a sudden drop from 13.25 to 13.54 in 2010 September it became brighter by 0.79 mag over a period of just three and a half months. As shown in the right

[11] We define the hardness ratio as $HR = (H - S)/(H + S)$ with S and H being the background corrected counts in the 0.3–1.0 and 1.0–10 keV bands, respectively.

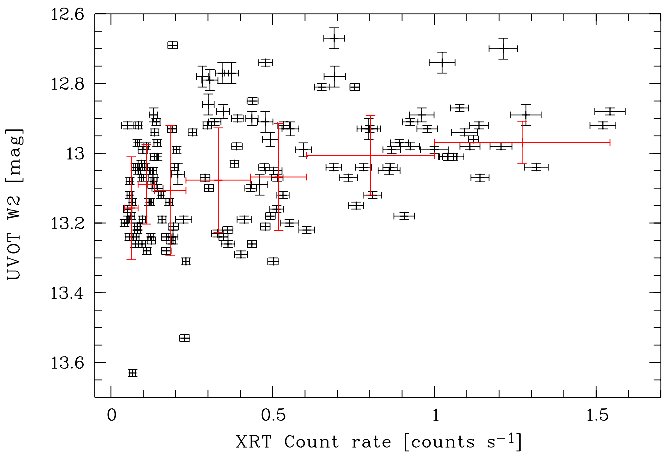

Figure 4. *Swift* XRT count rate vs. UVOT W2 magnitude. The red crosses correspond to bins in count rate containing 25 measurements and the mean UVOT W2 magnitude and standard deviation in that bin.

(A color version of this figure is available in the online journal.)

panel of Figure 2, it shows an even stronger drop between 2011 June and September. On 2011 June 11, it reached its brightest UV state seen during our entire *Swift* monitoring campaign with UVW2 = 12.69 mag. This brightening, however, was followed by a continuous fading in the W2 filter with the lowest measurement with 13.63 mag on 2011 September 9. This is a drop in W2 by almost 1 mag within three months, equivalent to an increase in flux by a factor of 2.5—one of the strongest changes in the UV observed in our entire AGN sample (Grupe et al. 2010), which even exceeds the UV variability seen in WPVS 007 (Grupe et al. 2007b, 2008b). These drops in the UV flux are extremely rare in NLS1s, which tend to show no or only little UV variability (e.g., Grupe et al. 2010). Now in 2012 January, Mkn 335 displays a very high flux in the UV again, peaking on January 18 with a magnitude of 12.67 in UV W2.

Figure 4 displays the relation between the XRT count rate and the UVOT W2 magnitude. This plot shows that Mkn 335 is only found to be faint in the UV when the AGN is faint in X-rays. However, it appears to be bright in the UV independently of the XRT count rate. We found a linear correlation coefficient $r_l = -0.376$ with a probability $P = 0.00020$ of a random result. A Spearman rank order test results in a correlation coefficient $r_s = -0.347$, $T_s = 3.50$ with a probability $P = 0.00072$ of a random result. However, there is not a direct correlation with the source being bright in the UV when it is also bright in X-rays. There is a large scatter in the UV W2 magnitude when the AGN appears to be X-ray faint. Note that the faintest and the brightest UV W2 magnitudes are both measured when Mkn 335 has a count rate less than 0.5 counts s^{-1}. The large scatter may suggest that the X-ray and UV emission generally do not vary together.

To explore this in more detail, we investigated potential lags in the variability of the *Swift* XRT count rate and the UVOT W2 filter data during the time period between 2007 May and 2011 July. Using the Bayesian framework (e.g., Gregory 2005; Albert 2009, for an introduction to Bayesian analysis) we created "synthetic" model count rates from the observed W2 magnitudes. We first transformed the magnitudes into relative fluxes and then applied a Gaussian bandpass filter in order to only retain variability on specific timescales of interest. For every timescale that was tested the same filter was also applied to the observed count rates. The filtered "synthetic" time series was free to be rescaled and shifted in flux, as well as translated in time. Overall, our model has four free parameters: time lag, flux offset and linear scaling factor, and width of the Gaussian used for the timescale of the bandpass filter. We assigned uniform prior probabilities within sensible parameter ranges for all parameters. Assuming normally distributed uncertainties, we then calculated the likelihood of obtaining the observed count rate data, given a particular set of parameter values for our model. Using the nested sampling code MultiNest (Feroz et al. 2009), we calculated the posterior probability distributions for all four parameters, as well as the Bayesian evidence. For comparison, we also calculated the Bayesian evidence for a reference model with constant flux (i.e., no information from the W2 magnitudes is used except for the temporal sampling). Our calculations show that the constant flux model is preferred over the model created from the W2 magnitudes. Therefore, we conclude that at present there is not enough evidence for lags between the XRT count rate and W2 filter for Mkn 355. A more detailed description of the method used, and its application to the Mkn 355 data, will be provided in an upcoming paper (M. Gruberbauer et al. 2012, in preparation).

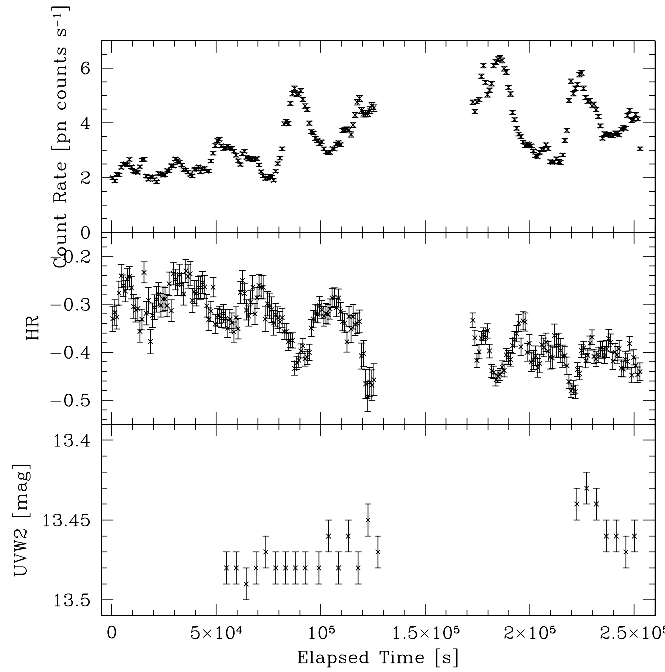

Figure 5. *XMM-Newton* pn and OM W2 light curves of Mkn 335 during the 2009 observation.

3.2. *Short-term Variability Observed by XMM-Newton*

Figure 5 shows the *XMM-Newton* EPIC pn count rate and hardness ratio and OM W2 light curves. The pn light curve was binned in 1000 s bins. The W2 bins are typically 4400 s as listed in Table 2. Overall, Mkn 335 appeared to be brighter during the 2009 June observation compared with the 2007 July observation (Grupe et al. 2007a). The overall trend is that the AGN becomes softer when the overall count rate increases from the beginning to the end of the *XMM-Newton* observations. Also note that the "flares" appear to be soft. These "flares" show doubling times of roughly 3 hr. This "flaring" is similar to what had been reported by O'Neill et al. (2007) during the 133 ks 2006 *XMM-Newton* high-state observation. The light curve from the 2006 *XMM-Newton* observation is displayed in Figure 6 for comparison.

The *XMM-Newton* 2009 pn light curve shown in Figure 5 suggests a dependence of the hardness ratio and therefore the

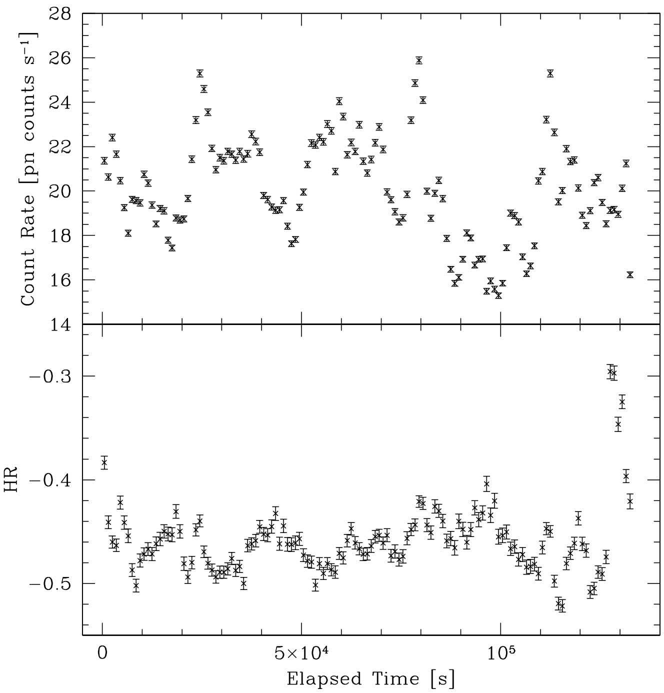

Figure 6. *XMM-Newton* pn light curves of Mkn 335 during the 2006 observation.

shape of the X-ray spectrum on count rate. Figure 7 displays the count rate versus hardness ratios in the 2009 and 2006 *XMM-Newton* observations in the left and right panels, respectively. Clearly, there is a strong correlation between count rate and hardness ratio in the low-state 2009 observation. A Spearman rank order test results in a correlation coefficient $r_s = -0.73$ with a Student's T-test value $T_s = -15.3$ with a probability of $P < 10^{-4}$ of a random result. However, the high-state data from 2006 give a completely different picture. Here we only see a marginal trend that the source becomes softer with increasing count rate. A Spearman rank order test results is $r_s = -0.20$, $T_s = -2.3$, and a probability $P = 0.023$.

The *Swift* long-term monitoring data confirm that there is only a strong correlation between the count rate and hardness ratio when the AGN is in the low state. This result is similar to the one found in the *XMM-Newton* data. During the high state (like in the 2006 *XMM-Newton* data), we do not see a dependence of the X-ray spectral shape with X-ray flux.

3.3. X-Ray Spectral Analysis

3.3.1. General Remarks

As shown in the previous subsection, Mkn 335 displays a strong dependence of the shape of its X-ray spectrum on its X-ray flux: the X-ray spectrum appears to be harder when Mkn 335 is in a low state and softer when in a bright state. Therefore, performing and interpreting the spectral fits to the average data set will be limited. We therefore split the data into "bright" and "faint" states, defining "bright" as phases when the pn count rate was >4 counts s^{-1} and "faint" when the count rate was <3 counts s^{-1}, corresponding to 0.2–10 keV fluxes of 1.6×10^{-14} and 1.2×10^{-14} W m $^{-2}$, respectively. This results in four spectra, one "bright" and "faint" in each of the two orbits. However, most relevant are the spectra of the "faint" state of the first orbit and the "bright" state of the second orbit. The other two spectra do not have enough quality to allow detecting significant spectral changes. Therefore, for the remainder of the paper we focus on these two epochs of the 2009 observation. The 2009 first orbit "faint" state and the second orbit "bright" state data are denoted (I) and (II) in Table 4. In addition, we have also included the low-state spectrum from 2007 July (Grupe et al. 2008a) to our analysis in order to investigate, if and how the overall spectral shape changed over those two years. This spectrum is marked as (III) in Table 4.

In order to see how much the spectra have changed between 2007 July when Mkn 335 was in its low state (Grupe et al. 2008a) and 2009 June, as a first step, we fitted the new data with the 2007 best-fit absorption model. The 2009 first orbit "faint" and second orbit "bright" mode were therefore described with a power-law model with Galactic and intrinsic partial covering absorption, fixed to the parameters determined for the 2007 low-state data with $N_{\rm H,pc} = 15.1 \times 10^{22}$ cm^{-2}, $f_{\rm pc} = 0.94$, and $\alpha_{\rm X} = 1.78$ (Grupe et al. 2008a). The absorber at $z = 0$ was fixed to the Galactic value (3.96×10^{20} cm^{-2}; Dickey & Lockman 1990) which we used for all fits. This fit is shown in the left panel of Figure 8 with the first orbit "faint" spectrum displayed in black, the "bright" second orbit spectrum in red, and the 2007 low-state spectrum in green. Clearly, there is a strong deviation of the 2009 data from the neutral partial covering absorber model used for the 2007 spectrum. This result suggests that the absorber and/or the intrinsic continuum spectrum must have changed significantly.

Therefore, in order to start exploring which model can best characterize the observed changes in the spectra, and which

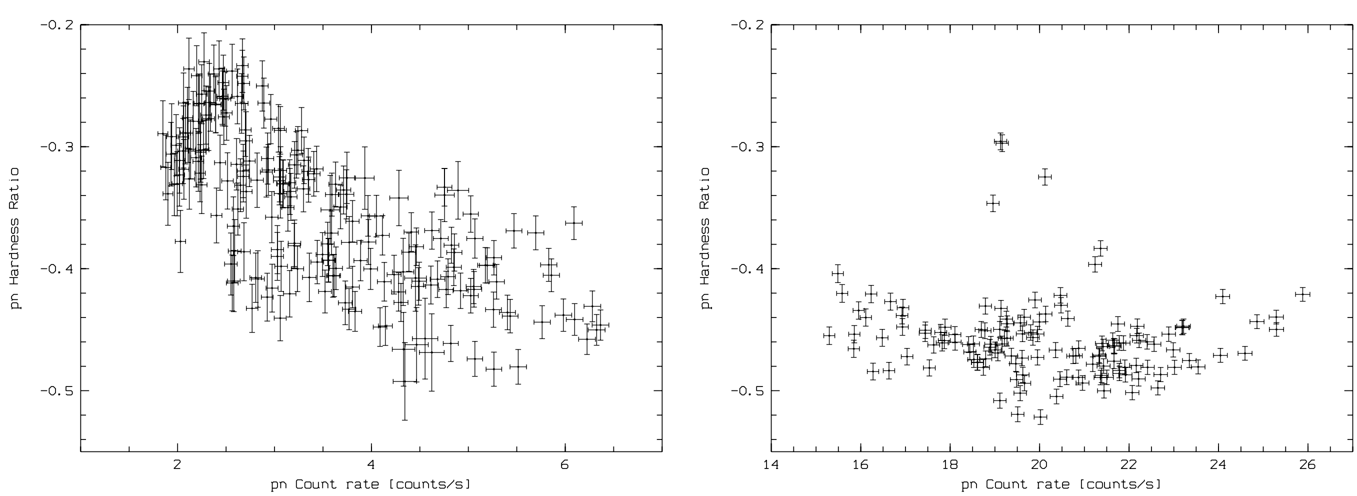

Figure 7. Count rate vs. hardness ratio of the 2009 (left) and 2006 (right) *XMM-Newton* observations.

Table 4
Results of the Spectral Fits to the "Faint" and "Bright" State *XMM-Newton* pn Data of Mkn 335 During the First and Second Orbit

Spectrum[a]	Model[b]	$\alpha_{X,soft}$	E_{break}	$\alpha_{X,hard}$	T_{BB}[c]	$N_{H,pc}$[d]	f_{pc}	$\log(\xi)$	χ^2/ν
(I)	powl	1.36 ± 0.01	...	...	...	...	...	...	4071/117
	bknpo	1.74 ± 0.02	1.27 ± 0.03	0.52 ± 0.02	...	...	...	...	198/115
	bb + po	...	...	0.52 ± 0.02	99 ± 2	...	...	...	209/115
	zpcfabs * po	1.65 ± 0.01	...	...	...	5.1 ± 0.2	0.78 ± 0.01	...	516/115
	zpcfabs * (bb + po)	...	...	$0.77^{+0.06}_{-0.12}$	97 ± 2	3.7 ± 1.0	$0.33^{+0.05}_{-0.13}$	...	191/113
	zxipcf * po	1.18 ± 0.01	...	...	...	5.75 ± 0.30	1.00^{f}	2.24 ± 0.02	255/114
	zxipcf * (bb + po)	...	...	$0.92^{+0.05}_{-0.10}$	110^{+3}_{-5}	10.5 ± 1.5	$0.51^{+0.05}_{-0.09}$	$1.91^{+0.05}_{-0.08}$	154/112
(II)	powl	1.55 ± 0.01	...	...	...	...	...	...	6749/135
	bknpo	1.86 ± 0.01	1.34 ± 0.02	0.73 ± 0.02	...	...	...	...	338/133
	bb + po	...	...	0.75 ± 0.01	97 ± 2	...	...	...	511/133
	zpcfabs * po	1.79 ± 0.01	...	...	...	5.5 ± 0.2	0.76 ± 0.01	...	838/133
	zpcfabs * (bb + po)	...	...	$1.11^{+0.04}_{-0.08}$	94 ± 1	$5.3^{+0.6}_{-0.5}$	$0.43^{+0.03}_{-0.08}$	...	429/131
	zxipcf * po	1.35 ± 0.01	...	...	...	5.95 ± 0.20	1.00^{f}	2.30 ± 0.02	439/132
	zxipcf * (bb + po)	...	...	1.12 ± 0.02	106^{+3}_{-2}	13.1 ± 1.2	0.51^{g}	1.91^{g}	245/132
(III)	zpcfabs * (bb + po)	...	...	1.44 ± 0.12	105^{+7}_{-6}	$13.5^{+1.1}_{-1.0}$	0.90 ± 0.02	...	136/87
	zxipcf *(bb + po)	...	...	$0.94^{+0.08}_{-0.09}$	113^{+10}_{-8}	$22.4^{+4.2}_{-1.6}$	$0.87^{+0.02}_{-0.03}$	2.06 ± 0.05	132/86
(I) + (II)	zpcfabs * (bb + po)	...	...	0.97 ± 0.05	95 ± 3	$5.6^{+1.0}_{-0.7}$	0.31 ± 0.04	...	647/246
						$6.0^{+0.6}_{-0.5}$	0.68 ± 0.02	$1.23^{+0.11}_{-0.24}$	
	zxipcf * (bb + po)	...	...	$1.17^{+0.04}_{-0.03}$	110 ± 3	13.5 ± 1.0	0.57 ± 0.03	$1.91^{+0.02}_{-0.03}$	406/244
						4.1 ± 0.4	0.53 ± 0.03		
(I) + (II) + (III)	zpcfabs * (bb + po)	...	...	1.04 ± 0.05	96 ± 3	$5.3^{+1.0}_{-0.7}$	0.37 ± 0.04	...	823/334
						12.8 ± 1.2	0.81 ± 0.02		
						$6.0^{+0.6}_{-0.5}$	$0.68^{+0.02}_{-0.01}$	$1.23^{+0.12}_{-0.21}$	
	zxipcf * (bb + po)	...	...	$1.17^{+0.04}_{-0.03}$	110 ± 3	13.5 ± 1.0	0.57 ± 0.03	1.91 ± 0.03	535/329
				1.00 ± 0.01	114 ± 1	$22.3^{+3.9}_{-1.5}$	0.88 ± 0.02	2.05 ± 0.05	

Notes.
[a] Spectra: (I) 2009, Orbit 1, faint; (II) 2009, Orbit 2, bright; (III) 2007.
[b] Spectra models—powl: single power law; bknpo: broken power law; bb: blackbody; zpcfabs: redshifted neutral partial covering absorber, zxipcf: ionized redshifted partial covering absorber; note that all models are fitted with the absorption model wabs with the column density fixed to the Galactic value of 3.96×10^{20} cm^{-2} taken from Dickey & Lockman (1990). For all models we excluded the energy ranges 0.45–0.6, 0.7–1.1, and 5.5–6.7 keV.
[c] The blackbody temperature T_{BB} is given in units of eV.
[d] The column density of the ionized partial covering absorber is given in units of 10^{22} cm^{-2}.
[e] The ionization parameter ξ is given in units 10^{-5} W m, or erg s^{-1} cm.
[f] The covering fraction of the ionized absorber pegged.
[g] Covering fraction and ionization parameter fixed to the values of the low state. When left as free parameters log ξ results in the same value, but f_{pc} is not constrained.

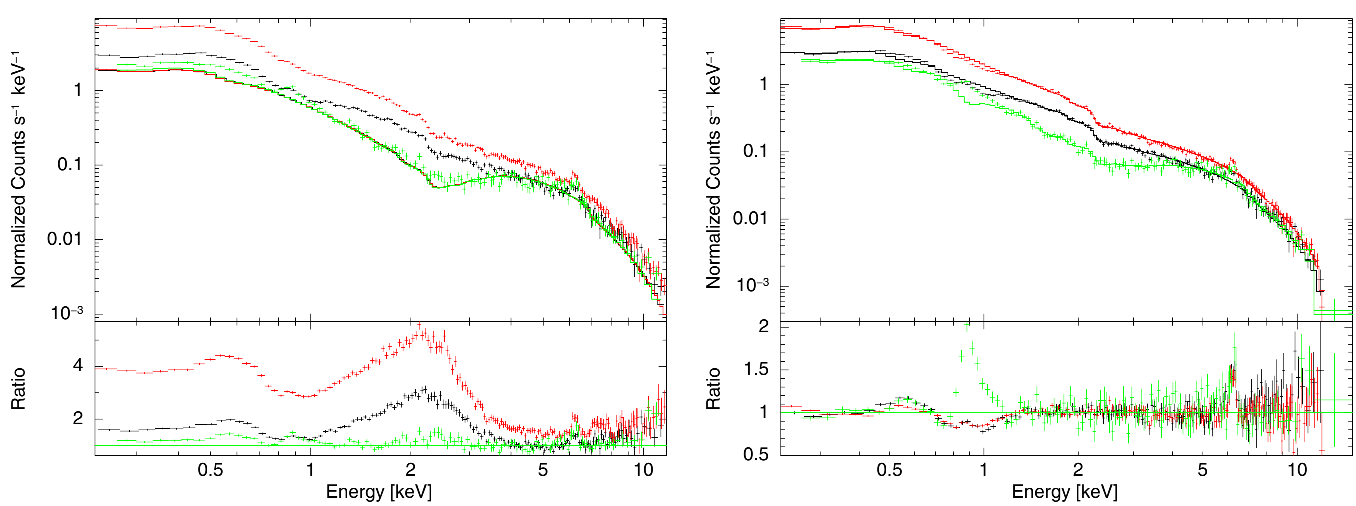

Figure 8. *XMM-Newton* 2009 first orbit "faint state," second orbit "bright state" and the pn 2007 low-state data of Mkn 335. The data are displayed in black, red, and green, respectively. In the left panel, the spectra were modeled by a neutral partial covering absorber model using the parameters as given in Grupe et al. (2008a); $N_{H,pc} = 15.1 \times 10^{22}$ cm^{-2}, $f_{pc} = 0.94$, $\alpha_X = 1.78$. In the right panel, the spectra were fitted with an ionized partial covering absorber and an underlying blackbody plus power-law spectrum as listed in Table 4.

(A color version of this figure is available in the online journal.)

models can be safely ruled out, in a second step we applied some simple spectral models to the new data; and we continue to compare with the previous data (note that those did not have simultaneous *deep* RGS observations). In these models, we fix and tie as many parameters as possible and then thaw them in order to study systematically the influence on the spectral fits of each of these parameters. There are strong residuals around 0.5, 0.9, and 6.4 keV, which are likely due to well-localized X-ray emission lines and absorption edges. In order to constrain the broadband continuum parameters, we excluded the energy ranges 0.45–0.6, 0.7–1.1, and 5.5–6.7 keV at first from further analysis at this point. These energy bands correspond to the O VII and O VIII emission lines and absorption edges, and the Fe Kα emission line complex. This strategy will keep the number of free parameters low and we can focus on the continuum properties first.

3.3.2. Simple Spectral Models

The results of five spectral fits are summarized in Table 4. We start with those simple models that have been routinely applied to essentially all AGNs observed so far: a single power law, a broken power law, a power law with soft excess, and a power law with absorption. First of all, we find that a single absorbed power-law model does not result in an acceptable fit for any of these spectra. Although a broken power-law model does significantly improve the fits, it is not an acceptable model for any of the spectra, either. The same holds true for a power law plus blackbody-type soft excess. Therefore, other models are required to describe the data, and we continue with the next most obvious addition: an ionized absorption component.

3.3.3. X-Ray Continuum Fits with Partial Covering Absorber Models

As a first step in characterizing the 2009 spectra, we used a power law with neutral partial covering absorber, as we successfully applied it to the 2007 low-state data. The absorption column density and the covering fraction were left free to vary. However, this model does not yield acceptable results for the 2009 data, neither when fitting the model to the single spectra, nor when fitting it simultaneously to the “faint state” of the first orbit and the “bright state” during the second orbit. The next step was to fit the spectra with an ionized partial covering absorber ($zxipcf$ in XSPEC as described by Reeves et al. 2008) and a power-law model. As shown in Table 4, the underlying intrinsic continuum spectrum cannot be modeled by a single power law and requires an extra component, but the addition of a blackbody component improves the fit. All spectra can be basically fitted with an intrinsic spectrum with the same blackbody temperature and a hard X-ray spectral slope $\alpha_X = 1.0$. When all parameters of the ionized partial covering absorber are left free to vary, all 2009 spectra show very similar covering fractions and ionization parameters. If we fix the covering fraction to 51% and the ionization parameter to $\log\xi = 1.91$ [10^{-5} W m, erg s^{-1} cm], then the differences in the spectra are mostly due to changes in the absorption column density of the ionized partial covering absorber.

In a final step, we fitted the 2009 “faint” and “bright” spectra and the 2007 low-state spectrum simultaneously, again with an ionized partial coverer. As shown in Table 4, the 2007 data can be fitted by the ionized partial covering absorber model. However, they are fully consistent with a neutral partial covering absorber model as well.

Given the possible degeneracy of the blackbody component and the parameters of the ionized absorber, further modeling and an accurate parameter determination of the absorber parameters is not possible with the CCD-type spectra discussed here. Therefore, no further modeling is presented here. In fact, our RGS analysis (M. Gruberbauer et al. 2012, in preparation) suggests that a *multi*-component absorber is preferred to fully characterize the ionized medium. We have demonstrated that fitting the CCD spectrum with a single warm absorber is sufficient and more complex models are not warranted statistically, and would not yield meaningful results.

3.3.4. Fits with Refection Models

Although the continuum can be fitted by an ionized absorber model quite well, the previous spectral data of Mrk 335 could also be described in terms of the blurred reflection model (e.g., Ross & Fabian 2005). For completeness, here, we briefly show that such a model can also explain the new 2009 data; but we leave a study of the full parameter space of possible models to a dedicated future study (L. C. Gallo et al. 2012, in preparation).

The initial model is the double reflector model used to interpret the 2007 X-ray weak state of Mrk 335 (Grupe et al. 2008a). The model considered the possibility of having the disk illuminated by two different primary emitters; for example, a compact emitter located close to the black hole and a second, more extended corona illuminating the disk at larger distances. In the 2007 low state the spectrum was described as being reflection dominated where the direct emission from the power-law component was significantly suppressed relative to the reflection component. An additional component required in the 2007 low state was emission from a distant ionized emitter (Grupe et al. 2008a; Longinotti et al. 2008). This was modeled using the vmekal model in XSPEC for a hot, diffuse gas. There were no obvious absorption features in the 2007 spectrum.

Here, the 2007 data and the 2009 data are fitted together with the model described above. We find that the primary difference in the continuum between 2007 and 2009 is the level of the power-law emitter. That is, the power law is more dominant in the 2009 date than in the 2007 low state. The ionized emitter remains constant in all three spectra and is consistent with being emitted from large distances. The apparent weakness of the emission spectrum in 2009 is attributed to the increased fraction of the power-law component in the X-ray band.

Residuals remain in the fit at approximately 1.5 keV. Considering contribution from a warm absorber as is evident in the RGS analysis (A. L. Longinotti et al. 2012, in preparation) improves the fit. In an upcoming work, we are examining this model in much greater detail by considering also the variability of the source during each observation.

3.3.5. Fe Kα Emission

So far, the energy bins including the Fe Kα emission line energy range had been excluded from spectral fitting. The rest frame 6.4 keV Fe Kα line is present in all spectra. The width of the line is about $\sigma = 140$ eV. In order to determine the flux and equivalent width of the Fe Kα line during each observation, we fitted the spectra with a single power law plus redshifted Gaussian line in the 2–10 keV energy range. We found that the line fluxes determined from the 2009 “faint” and “bright” state and 2007 low-state spectra are $(9.6 \pm 2.2)\times10^{-17}$ W m^{-2}, $(12.9 \pm 2.4)\times10^{-17}$ W m^{-2}, and $(13.2 \pm 3.3)\times10^{-17}$ W m^{-2}, respectively. These fluxes suggest that the line has been constant regardless in which state the AGN is. The equivalent widths were 220 ± 75, 200 ± 60, and 310 ± 110 eV, respectively. The values for the narrow Fe Kα line are very similar when the reflection model is applied to the data.

4. DISCUSSION AND CONCLUSIONS

We presented the results from our long-term monitoring campaign with *Swift* and the short-term light-curve and X-ray spectral analysis of the highly variable NLS1 Mkn 335 using a dedicated, triggered 200 ks observation with *XMM-Newton*. Mkn 335 is one of the best examples of a typically bright AGN that goes through states of low X-ray fluxes. Another example is the Seyfert 1 PG 0844+349 for which we recently reported on an *XMM-Newton* observation during its deep low X-ray flux state (Gallo et al. 2011). After Mkn 335 was discovered in an extremely low X-ray flux state in 2007 May, we discovered in the 20 ks *XMM-Newton* observation from 2007 July that it showed strong soft X-ray emission lines (Grupe et al. 2008a). This observation however was too short to put constraints on the ionized gas properties and to model the continuum shape of the low state in detail. Therefore, we triggered the deep *XMM-Newton* observation discussed here, which also led to the first detection of narrow absorption lines in Mkn 335 with RGS (A. L. Longinotti et al. 2012, in preparation).

4.1. Continuum Spectrum

As we saw previously for the 2007 low-state *XMM-Newton* observations of Mkn 335, partial covering absorber and reflection models yield a similar quality of the spectral fits. The continuum spectrum is highly variable and complex. When Mkn 335 was observed by *XMM-Newton* in 2009 June it varied very fast on timescales of just hours with the spectrum becoming softer with increasing X-ray flux. The 2009 data require that the absorber has to be ionized. Since there were no signs of intrinsic absorption features in the 2000 and 2006 *XMM-Newton* and *Suzaku* data, the presence of the absorber is not permanent, but transient.

How is a partial coverer model consistent with the long-term variability behavior of this NLS1 seen by *Swift*? As shown in Sections 3.1 and 3.2 the X-ray spectra become softer with increasing X-ray flux. At first glance, an increase in flux could mean intrinsically an increase of the accretion rate and therefore luminosity and $L/L_{\rm Edd}$ which would result in a steeper X-ray spectrum (Grupe 2004; Grupe et al. 2010; Shemmer et al. 2008). However, as we have seen from the shape of the X-ray spectrum, this simple picture cannot explain the X-ray spectrum which is much more complicated than a simple power-law model. A variable partial covering absorber, however, can explain the X-ray light curves seen on long as well and short timescales: When the absorber becomes stronger and the observed X-ray flux lower, the spectrum becomes harder. On the other hand, when the absorber becomes more transparent or even disappears the spectrum becomes soft.

4.2. X-Ray Variability

As we have shown in Figures 1, 5, and 6, Mkn 335 is highly variable in X-rays on long and short timescales. Our long-term *Swift* monitoring has shown that Mkn 335 varies in X-rays by factors of about 40 even within months. Beside this strong flux variability we also observe a strong spectral variability when the AGN is in a low state. Above a certain threshold we only see X-ray flux variability with no significant changes in the hardness ratio. This behavior appears on short as well as on long timescales (see Figures 3 and 7). Such a behavior has also been reported by Turner et al. (2008, 2011) for NGC 3516. If we assume the partial covering absorber picture, then the spectral changes in the hardness ratio at lower X-ray fluxes can be explained in terms of changes in the absorber properties, such as the column density, covering fraction, and ionization parameter.

Indeed, we find that the flux in the Fe Kα line is constant, regardless of the state of the AGN. This constant line flux indicates an underlying continuum component that is not variable.

4.3. UV Variability

The UV light curve of Mkn 335 is quite remarkable. While NLS1s typically vary by only 0.3 mag in the UV (Grupe et al. 2010), Mkn 335 shows variability by about 1 mag over a timescale of a few months as seen between 2010 September and December and 2011 June and September. (The strongest UV variability we have seen from the *Swift* observations listed in Grupe et al. (2010) was from Seyfert 1.5 galaxies.) In Mkn 335, we did not find any clear correlation between the X-ray and UV flux changes. This result may suggest that the changes in the UV flux are not directly linked to changes in the X-ray flux. However, as shown in the *XMM-Newton* short-term light curve (Figure 5) the brightening in the OM W2 light curve at the end could be seen as a response to the "flare" at 225 ks in X-rays. Currently, we do not have the temporal resolution to exclude that there is not a direct connection between the UV and X-rays. Our investigation of possible lags between the UV and X-ray emission is certainly affected by the undersampling in the *Swift* light curves. As we have seen from the *XMM-Newton* 2009 light curve, Mkn 355 is highly variable even on timescales of hours. Our current *Swift* light curve systematically undersamples these timescales.

4.4. Mkn 335 and AGNs in Deep Minimum X-Ray Flux States

Mkn 335 is one of the best examples of an AGN that used to be typically in an X-ray bright flux state but then suddenly became dramatically fainter. The most extreme of these cases is the NLS1 WPVS 007 (Grupe et al. 1995) which dropped by a factor of more than 400 between its *ROSAT* All-Sky Survey (RASS; Voges et al. 1999) and *ROSAT* pointed observations about three years later. *FUSE* UV spectroscopy and *Swift* X-ray observations revealed the presence of strong UV absorption line troughs and a partial covering absorber in X-rays (Leighly et al. 2009; Grupe et al. 2008b). In the case of WPVS 007, our interpretation is that this is a low-luminosity, low-redshift analogon of a broad absorption line quasar (BAL QSO) as suggested by Leighly et al. (2009). Because the black hole mass in WPVS 007 is only a few 10^6 $M_\odot$, the timescales in this AGN are hundreds of times shorter than in a typical BAL QSO. Mkn 335 could be just another example of such a BAL QSO analogons. As pointed out by Brandt & Gallagher (2000) and Boroson (2002), BAL QSOs and NLS1s are both AGNs with high $L/L_{\rm Edd}$ Eddington ratios, but with significantly different central black hole masses. WPVS 007 as well as Mkn 335 may be the link between these two AGN classes.

4.5. Conclusions

We presented the results from a more than four-year long monitoring campaign with *Swift* of the NLS1 Mkn 335, one of the longest with simultaneous X-ray and UV measurements so far obtained for an AGN. We also presented a 200 ks observation with *XMM-Newton* triggered at low-flux state. We found that:

1. Mkn 335 continues to be highly variable in X-rays on long and short timescales. The total amplitude of variability in count rate in the *Swift* XRT data (peak to dip between 2007 and 2011) is a factor of 24. The lowest count rate was seen on 2011 August 28 with 0.042 counts s^{-1} and the highest count rate on 2007 October 18 with 1.277 counts s^{-1}. The fastest doubling timescale we saw from the *XMM-Newton* observation in 2009 was about 2 hr during the first orbit making it one of the most rapidly varying AGNs in X-rays.
2. The X-ray and UV variability is not strongly correlated. However, during X-ray bright states, the faintest UV states do not occur, while during X-ray low states the amplitude of UV variability is highest.
3. With a variability of about 1 mag in the UV within a few months as seen between 2011 June and September, Mkn 335 is one of the most variable NLS1 known in the UV.
4. Its X-ray hardness ratio shows distinct variability patterns in high and low states. During the low states, there is a clear correlation of hardness ratio with count rate. However, this pattern disappears in high state; hardness ratio is independent of count rate, and occasionally shows some abrupt changes on short timescales.
5. Formally, both ionized absorbers and blurred reflectors do provide successful spectral fits to the *XMM* low-state data.

While the presence of ionized absorption is confirmed by the RGS data (M. Gruberbauer et al. 2012, in preparation), the number and the properties of all spectral components present at any given time will be addressed by in-depth follow-up modeling. Mrk 335 continues to be one of the few AGNs which are still bright enough in their low states for spectral analysis, and therefore hold the best hopes of understanding AGN spectral components, spectral complexity, and mechanisms of variability. We continue to monitor Mrk 335, in order to identify pronounced high and low states.

We thank the *Swift* PI Neil Gehrels for approving our various ToO requests to monitor Mkn 335 with *Swift*, and the *XMM-Newton* Science Operations Team for their fast turn around when we requested our 200 ks triggered observation. Many thanks also to the anonymous referee for useful comments and suggestions. We acknowledge the use of public data from the *Swift* data archives. This research has made use of the NASA/IPAC Extragalactic Database (NED) which is operated by the Jet Propulsion Laboratory, Caltech, under contract with the National Aeronautics and Space Administration. This research has made use of the XRT Data Analysis Software (XRTDAS) developed under the responsibility of the ASI Science Data Center (ASDC), Italy. S.K. acknowledges the hospitality of the Aspen Center for Physics, and thanks the participants for discussions on AGN X-ray spectral models. D.X. and S.K. acknowledge support from the Chinese National Science Foundation (NSFC) under grant NSFC 10873017. D.X. also acknowledges support from program 973 (2009CB824800). *Swift* is supported at PSU by NASA contract NAS5-00136. This research was supported by NASA contracts NNX08AT25G, NNX09AP50G, and NNX09AN12G (D.G.).

REFERENCES

Albert, J. 2009, Bayesian Computation with R (Dordrecht: Springer)
Arevalo, P., McHardy, I. M., & Summons, D. P. 2008, MNRAS, 388, 211
Arnaud, K. A. 1996, in ASP Conf. Ser. 101, Astronomical Data Analysis Software and Systems V (San Francisco, CA: ASP), 17
Ballantyne, D. R., Iwasawa, K., & Fabian, A. C. 2001, MNRAS, 323, 506
Ballo, L., Giustini, M., Schartel, N., et al. 2008, A&A, 483, 137
Boroson, T. A. 2002, ApJ, 565, 78
Brandt, W. N., & Gallagher, S. C. 2000, New Astron. Rev., 44, 461
Breeveld, A. A., Curran, P. A., Hoversten, E. A., et al. 2010, MNRAS, 406, 1687
Burrows, D., Hill, J. E., Nousek, J. A., et al. 2005, Space Sci. Rev., 120, 165
Cardelli, J. A., Clayton, G. C., & Mathis, J. S. 1989, ApJ, 345, 245
Chevalier, L., Collins, S., Dumont, A.-M., et al. 2006, A&A, 449, 493
den Herder, J. W., Brinkman, A. C., Kahn, S. M., et al. 2001, A&A, 365, L17
Dickey, J. M., & Lockman, F. J. 1990, ARA&A, 28, 215
Fabian, A. C., Ballantyne, D. R., Merloni, A., et al. 2002, MNRAS, 331, L35
Fabian, A. C., Miniutti, G., Gallo, L. C., et al. 2004, MNRAS, 353, 1071
Fabian, A. C., Zoghbi, A., Ross, R. R., et al. 2009, Nature, 459, 540
Feroz, F., Hobson, M. P., & Bridges, M. 2009, MNRAS, 398, 1601
Gallo, L. C. 2006, MNRAS, 368, 479
Gallo, L. C., Grupe, D., Schartel, N., et al. 2011, MNRAS, 412, 161
Gehrels, N., Chincarini, G., Giommi, P., et al. 2004, ApJ, 611, 1005
George, I. M., Turner, T. J., Yaqoob, T., et al. 2000, ApJ, 531, 52
Godet, O., Beardmore, A. P., Abbey, A. F., et al. 2009, A&A, 494, 775
Gondoin, P., Orr, A., Lumb, D., & Santos-Lleo, M. 2002, A&A, 388, 74
Gregory, P. C. 2005, ApJ, 631, 1198
Grier, C. J., Peterson, B. M., Pogge, R. W., et al. 2012, ApJ, 744, L4
Grupe, D. 2004, AJ, 127, 1799
Grupe, D., Beuermann, K., Mannheim, K., et al. 1995, A&A, 300, L21
Grupe, D., Komossa, S., & Gallo, L. 2007a, ApJ, 668, L111
Grupe, D., Komossa, S., Gallo, L. C., et al. 2008a, ApJ, 681, 982
Grupe, D., Komossa, S., Leighly, K. M., & Page, K. L. 2010, ApJS, 187, 64
Grupe, D., Leighly, K. M., & Komossa, S. 2008b, AJ, 136, 2343
Grupe, D., Mathur, S., & Komossa, S. 2004a, AJ, 127, 3161
Grupe, D., Schady, P., Leighly, K. M., et al. 2007b, AJ, 133, 1988
Grupe, D., Thomas, H.-C., & Beuermann, K. 2001, A&A, 367, 470
Grupe, D., Wills, B. J., Leighly, K. M., & Meusinger, H. 2004b, AJ, 127, 156
Halpern, J. P. 1982, PhD thesis, Harvard Univ.
Hill, J. E., Burrows, D. N., Nousek, J. A., et al. 2004, Proc. SPIE, 5165, 217
Jansen, F., Lumb, D., Altieri, B., et al. 2001, A&A, 365, L1
Larsson, J., Miniutti, G., Fabian, A. C., et al. 2008, MNRAS, 384, 1316
Leighly, K. M. 1999, ApJS, 125, 317
Leighly, K. M., Halpern, J. P., Jenkins, E. B., et al. 2007, ApJ, 663, 103
Leighly, K. M., Hamann, F., Casebeer, D. A., & Grupe, D. 2009, ApJ, 701, 176
Longinotti, A. L., Bianchi, S., Ballo, L., de la Calle, I., & Guainazzi, M. 2009, MNRAS, 394, L1
Longinotti, A. L., Nucita, A., Santos-Lleo, M., & Guainazzi, M. 2008, A&A, 484, 311
Longinotti, A. L., Sim, S. A., Nandra, K., & Cappi, M. 2007a, MNRAS, 374, 237
Longinotti, A. L., Sim, S. A., Nandra, K., Cappi, M., & O'Neill, P. 2007b, in ASP Conf. Ser. 373, The Central Engine of Active Galactic Nuclei, ed. L. C. Ho & J.-M. Wang (San Francisco, CA: ASP), 341
Mason, K. O., Breeveld, A., Much, R., et al. 2001, A&A, 365, L36
Merloni, A., Malzac, J., Fabian, A. C., & Ross, R. R. 2006, MNRAS, 370, 1699
Miller, L., Turner, T. J., & Reeves, J. N. 2008, A&A, 483, 437
Miller, L., Turner, T. J., & Reeves, J. N. 2009, MNRAS, 399, L96
Miller, L., Turner, T. J., Reeves, J. N., et al. 2007, A&A, 463, 131
Miniutti, G., Fabian, A. C., Brandt, W. N., Gallo, L. C., & Boller, T. 2009, MNRAS, 396, L85
Nandra, K., & Pounds, K. A. 1994, MNRAS, 268, 405
O'Neill, P. M., Nandra, K., Cappi, M., Longinotti, A. L., & Sim, S. A. 2007, MNRAS, 381, L94
Peterson, B. M., Ferrarese, L., Gilbert, K. M., et al. 2004, ApJ, 613, 682
Poole, T. S., Breeveld, A. A., Page, M. J., et al. 2008, MNRAS, 383, 627
Pounds, K. A., Stanger, V. J., Turner, T. J., King, A. R., & Czerny, B. 1987, MNRAS, 224, 443
Reeves, J., Done, C., Pounds, K., et al. 2008, MNRAS, 385, L108
Risaliti, G., Salvati, M., Elvis, M., et al. 2009, MNRAS, 393, L1
Roming, P. W. A., Kennedy, T. E., Mason, K. O., et al. 2005, Space Sci. Rev., 120, 95
Roming, P. W. A., Koch, T. S., Oates, S. R., et al. 2009, ApJ, 690, 163
Ross, R. R., & Fabian, A. C. 2005, MNRAS, 358, 211
Schartel, N., Rodríguez-Pascual, P. M., Santos-Lleó, M., et al. 2007, A&A, 474, 431
Schartel, N., Rodríguez-Pascual, P. M., Santos-Lleó, M., et al. 2010, A&A, 512, 75
Schlegel, D. J., Finkbeiner, D. P., & Davis, M. 1998, ApJ, 500, 525
Shemmer, O., Brandt, W. N., Netzer, H., Maiolino, R., & Kaspi, S. 2008, ApJ, 682, 81

Strüder, L., Briel, U., Dennerl, K., et al. 2001, A&A, 365, L18
Tanaka, Y., Nandra, K., Fabian, A. C., et al. 1995, Nature, 375, 659
Tananbaum, H., Peters, G., Forman, W., et al. 1978, ApJ, 223, 74
Turner, M. J., Abbey, A., Arnaud, M., et al. 2001, A&A, 365, L27
Turner, T. J., & Miller, L. 2009, A&AR, 17, 47
Turner, T. J., Miller, L., Kraemer, S. B., & Reeves, J. N. 2011, ApJ, 733, 48
Turner, T. J., Miller, L., Reeves, J. N., & Kraemer, S. B. 2007, A&A, 475, 121
Turner, T. J., Nandra, K., Zdziarski, A. A., et al. 1993, ApJ, 407, 556
Turner, T. J., Reeves, J. N., Kraemer, S. B., & Miller, L. 2008, A&A, 483, 161
Vignali, C., Piconcelli, E., Bianchi, S., & Miniutti, G. 2008, MNRAS, 388, 761
Voges, W., Aschenbach, B., Boller, T., et al. 1999, A&A, 349, 389